Chapter 2

New Optical Techniques For Measurement

This chapter discusses the optical measurement techniques developed. Three new methods have been developed for measurement of diffusion co-efficient in transparent liquid solution using Michelson interferometer, Multiple beam interferometer and Artificial fringe projection. A method for measuring the hairiness of textile yarns using scattered light is also discussed. The last section of this chapter discusses a new method for phase transition studies of liquid crystals.

2.1 Diffusion Studies of Transparent Liquid Solutions

Diffusion is the movement of molecules due to their thermal energy under the influence of concentration gradient. During its movement, when a molecule collides with other molecules, its direction and speed changes. The rate of diffusion movements depends on the number of collisions between molecules. The process continues until uniformity of concentration is reached, or in other words, a state of equilibrium has been achieved. Here equilibrium is defined as a state of uniform concentration in which no diffusion occurs though the molecules are in continuous thermal motion. So, the diffusion is the net movement of molecules from a region of higher concentration to the region of lower concentration without help of any external force at a fixed temperature and pressure.

When the movement of the molecules occurs with the help of an external force, it is called convective flow or bulk flow and the process is called eddy diffusion[26]-[28]. Diffusion is the most fundamental property of any chemical system because of its mass transfer correlations. The rate of diffusion in the solid, liquid, and gas or vapor phases depends on the density and the mobility of the phases. Density indicates the total number of the molecules that can exist at the interface and how fast diffusion can take place within a phase while the mobility indicates the case in which a sample can be stirred or turbulence be caused within it[29]. In solids, diffusion occurs at a slow rate due to slow molecular motion because of the high density and limited mobility which is about 10^{-5} cm/min. In liquids, the molecular motion is more rapid because of lower density and greater mobility; hence the rate of diffusion is higher, which is about 0.05 cm/min. The molecular motion in gases or vapors is much more rapid owing to much lower density and greater mobility and hence the rate of diffusion is higher which is about 10 cm/min.

2.1.1 Importance of diffusion

The study of diffusion is important in chemical engineering as well as in other fields such as biological systems, pollution control and separation of isotopes. Diffusivity is an important parameter for the design of chemical equipment and is needed for mass transfer studies[17, 18, 30]. The knowledge of the transport properties of fluids, i.e. the viscosity, diffusivity and thermal conductivity is frequently required for designing new technological processes and also in research. On the other hand, knowledge of the diffusion coefficient is also required for the design of different process equipments used in chemical reactors for extraction, absorption and distillation. During a mass transfer study, the composition dependence of the diffusion coefficient is essential. This information is particularly needed for a proper design and rational operation of the separation of equipments[31].

Accurate experimental diffusion coefficients are of considerable use in checking various theories of liquid state, as well as for studies on the mechanism of mass transfer. In addition, knowledge of liquid diffusion coefficient increases the understanding of the

transport processes in liquids. In engineering practice, the diffusion coefficient is one of the important parameters for mass transfer correlations such as Schmidt number and Sherwood number[32]

The liquid phase diffusion coefficients are important for the testing of models for the liquid state and for calculating the mass transfer rates in various heat and mass transfer processes. They are also the fundamental parameters in the kinetics of certain reactions, which are diffusion controlled. For high temperature applications such as multiphase chemical reactors, the need for data particularly on diffusion is acute[33].

The existing data on the subject of diffusion are often inconsistent and can seldom be compared with another. This can be attributed in part to the different conditions applied, the varying degrees of errors as well as the diffusion process itself, which at best is slow and can easily be masked by thermal or mechanical convection. Diffusion coefficients can be obtained either experimentally or using empirical correlations. But the empirical correlations fail at high concentrations leading to the necessity of experimental methods which can give accurate results. Many physical and chemical methods are employed for finding the diffusivity experimentally with their characteristic advantages and disadvantages[30].

Diffusion coefficients in liquids is around 10^{-5} cm^2 sec which cannot be reliably estimated. This is true for common organic solvents, mercury and even molten iron. Exceptions occur for high molecular weight solutes like albumin and polystyrene, where diffusion can be 100 times more. The empirical correlations are limited to infinitely dilute solutions. In fact, the diffusion coefficients in liquids vary with solute concentrations, frequently by several percentage and with a maximum and minimum value. Some means of estimating these concentration dependent diffusion coefficients are needed[17].

One of the important experimental methods to determine diffusivity of transparent liquids is optical techniques. Light beam passing through a non uniform refractive index medium will undergo different optical path lengths at different positions. Optical methods to measure diffusion therefore depend upon the measurement of refractive index variation due to diffusing liquid solutions.

2.1.2 Optical methods for determination of diffusivity

Optical methods for measuring diffusion coefficient are classical interferometric methods which includes Jamin, Mach-Zehnder, Rayleigh and Gouy interferometers. Rayleigh and Gouy interferometry are considered as most precise methods to measure diffusion of liquid solutions[34]-[36]. One of the important optical techniques is holographic interferometry. Bochner and Pipman developed a method to measure diffusion of transparent liquid solution using double exposure holographic interferometry[37]. The diffusivity is deduced from simple and direct measurement of interferograms. This method is later used by Szydlowska & Janowska and Gray & Fenichel[38, 39]. A detailed mathematical treatment of holographic method is given by Ruiz-Betvia et al where a real time technique is used[40]. The advent of CCD camera made the recording of interference pattern very easy Marquardt et al used change in interference pattern due to variation in refractive index to determine the diffusivity value using a CCD camera[41]. D Paoletti et al developed a method for diffusivity measurement using Sandwich holography[42]. Digital speckle pattern interferometry (DSPI) can also be used for diffusivity measurements[43]-[45]. Ambrosini et al developed speckle decorrelation method to study diffusivity[46]. A scan laser beam interferometer was used by Alanis et al and Francini et al[47, 48]. Rashidnia and Balasubramanian developed a common path interferometer technique for diffusion coefficient measurement[49]. Recently a very simple method to measure diffusion coefficient using digital moiré was developed by Spagnolo et al[50].

But most of the above mentioned methods require very stringent optical conditions and are not easy to implement in industrial environment, where they are supposed to be used. So there is a scope for new methods for diffusivity measurement, which should be both accurate and simple. This section discusses some new optical methods to study unsteady diffusion process in transparent binary liquid solution. The methods use Michelson Interferometer, Multiple Beam Interferometer and White light with an artificially produced fringe pattern.

2.1.3 Chemical System Investigated

Ammonium Dihydrogen Phosphate solution is used for testing. It is an important constituent of mixed fertilizers. The knowledge of the physicochemical properties of the solution of this salt is useful in interpreting the behavior of supplying nutrients and also diffusivity data of this system is very useful in prediction of its mass transfer rates in dissolution and crystallization. Ammonium Dihydrogen Phosphate is chosen as it gives a transparent solution when dissolved in water.

2.1.4 Preparation of Solution

100 ml aqueous solution is prepared by dissolving the solute in distilled water. Amount of solute added for required concentration is given in Table 2.1 along with the refractive indices of each solution. Viscosities of these solutions at different temperatures were determined using Ubbelhode Viscometer (Model-AVS 350, Scott Gerate Gmbh, Germany), for the conversion of diffusion coefficients from one temperature to another. Fig. 2 1 shows the variation of refractive index with concentration for the Ammonium Dihydrogen Phosphate. Specifications for Ammonium Dihydrogen Phosphate are given in Appendix A

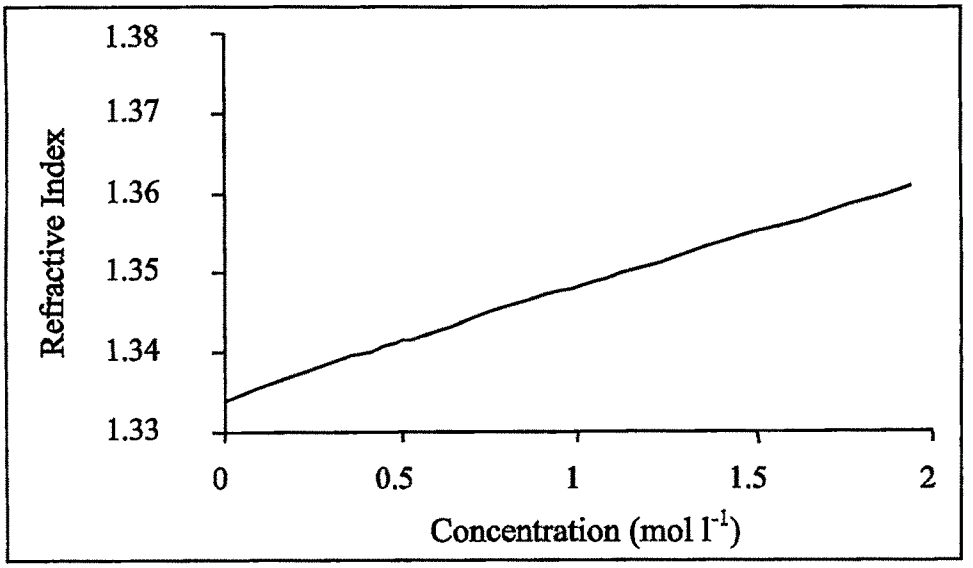

Figure 2.1: Change in refractive index with concentration

Table 2.1: Preparation of solutions and refractive index data for experimental runs

No	Concentration mol l^{-1}	gm solute/100 ml of solution	Refractive index
1	0.0000	0.0000	1.334
2	0.4484	5 1575	1 341
3	0.5479	0.3027	1.342
4	0.9461	10 8829	1.348
5	1 0456	12 0277	1.349
6	1.9409	22.3262	1 361
7	2.0405	23.4717	1.362
8	2.4512	28.1965	1.368
9	2.5463	29.2897	1.369

2.1.5 Experimental Cell

The experimental Cell was made up of crown glass having refractive index 1.51. The size of Experimental Cell was 2 5 $\times$ 2.5 $\times$ 5 cm^3, with the longer dimension along the diffusion direction. Two sides of the cell is painted black to avoid stray light entering the cell.

2.1.6 Cell Filling Procedure

The cell filling assembly and the cell are shown in the Fig.2.2. Lighter fluid was put in the cell with the help of a pipette; the cell is half filled with this solution. Denser solution having volume equal to half of the cell is put in the funnel. Using a control valve and a capillary tube, the denser fluid is put under the lighter fluid to lift it upwards. Filling procedure is monitored for any convection currents and flow rate

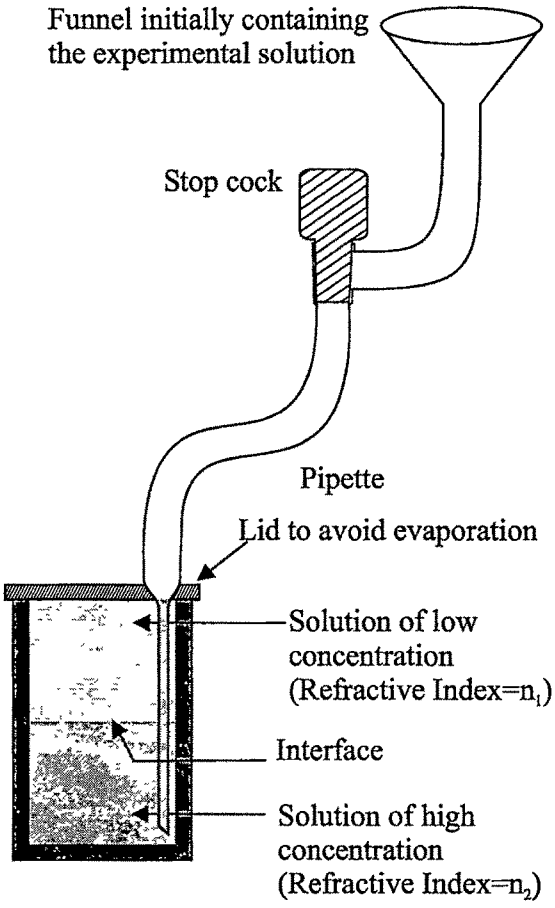

Figure 2.2: Cell filling apparatus

was adjusted to avoid them. Experiments are rejected when convection currents are observed. The cell is filled up to 2 mm below the overflow level to avoid overflow of solution on the glass windows of the cell and disturbing windows of the cell and the measurements Room temperature is measured for each experimental run.

2.1.7 Theory of diffusion

The process of diffusion starts after the cell is filled. Free diffusion process in an isothermal binary system is governed by Fick's second law and for one dimensional diffusion along x axis it is given by[51]-[53],

$$\frac{dC(x,t)}{dt} = D\frac{d^2C(x,t)}{dx^2} \tag{2.1}$$

where $C(x,t)$ is the concentration at position x and time t, D is the diffusion coefficient and x is the direction of diffusion. The solution of Eqn. (2.1) for two binary liquid mixtures initially ($t = 0$) separated at $x = 0$ with concentrations C_1 and C_2 is an error function and is[51],

$$C(x,t) = \frac{C_1 + C_2}{2} + \frac{C_2 - C_1}{2} \operatorname{erf}\left(\frac{x}{2\sqrt{Dt}}\right) \tag{2.2}$$

The error function is defined by[54],

$$\operatorname{erf}(u) = \frac{2}{\sqrt{\pi}} \int_0^u e^{-\eta^2}\, d\eta \tag{2.3}$$

The experiments are conducted for the range of concentration inside the diffusion cell The refractive index is a linear function of concentration (Fig. 2.1) and can be written as[55],

$$n(x,t) = m\, C(x,t) + n_0 \tag{2.4}$$

where $m = (dn/dC)_0$ is the mean value of the derivative for the applied concentration range and n_0 is a constant. A plot of variation in refractive index with diffusion direction (position inside the cell) at different instances of time is shown in Fig. 2 3. The plots were drawn using the concentration values of the solutions used in the experiments $C_{avg} = (C_1 + C_2)/2 = 0.9959$ mol l^{-1}. As the diffusion process progresses, the concentration and hence the refractive index changes. The medium inside the cell can be considered made up of layers perpendicular to diffusion direction having different refractive indices, which changes with time. This change in refractive index for two different instances of time t_1 and t_2 ($t_2 > t_1$) is given by,

$$\begin{aligned} \Delta n(x, t_1, t_2) &= n(x, t_2) - n(x, t_1) \\ &= m \frac{C_2 - C_1}{2} \left[\operatorname{erf}\left(\frac{x}{2\sqrt{Dt_2}}\right) - \operatorname{erf}\left(\frac{x}{2\sqrt{Dt_1}}\right)\right] \end{aligned} \tag{2.5}$$

The plot of position Vs Δn will have two characteristic extremes. This plot is shown in Fig 2.4 for two time intervals (30-45 min and 30-360 min) and the plot has two extremes x_1 and x_2 respectively for average concentration of 0.9959 mol l^{-1} (The MATLAB codes for the refractive index calculations are given in Appendix B.1 and B.2). These positions can be found from the condition,

$$\frac{\partial}{\partial x} \Delta n(x, t_1, t_2) = 0 \tag{2.6}$$

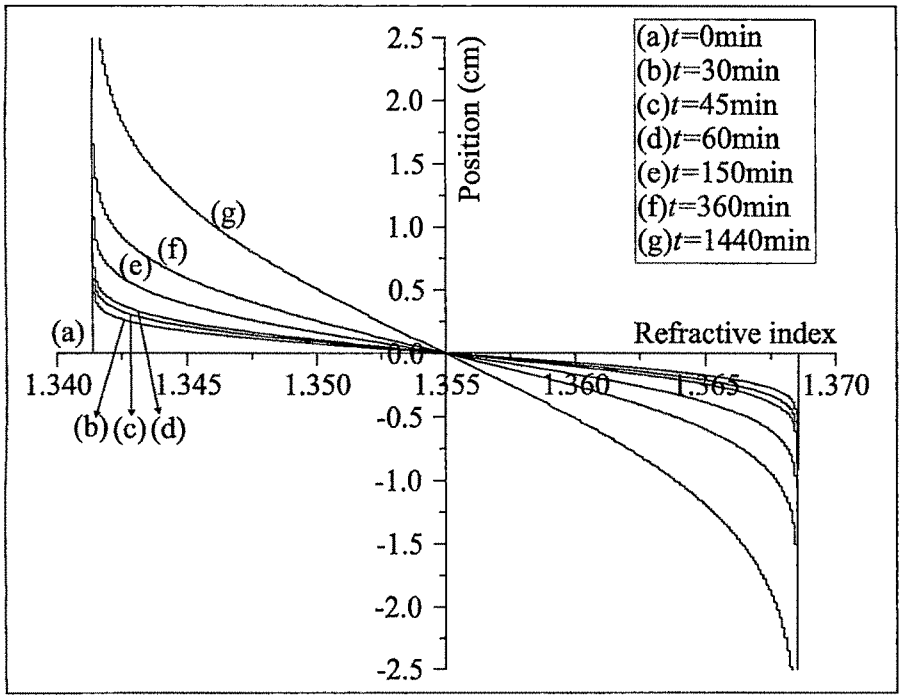

Figure 2.3: Change in refractive index with position

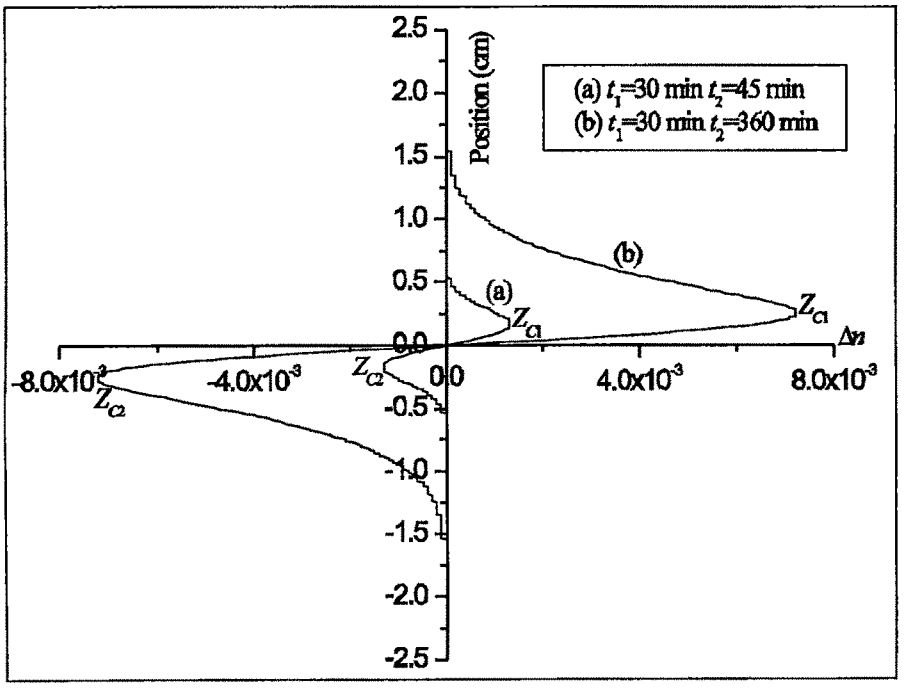

Figure 2.4: Change in Δn with position

$$i\,e.\quad \frac{\partial}{\partial x}\left(\operatorname{erf}\left[\frac{x}{2\sqrt{Dt_2}}\right]-\operatorname{erf}\left[\frac{x}{2\sqrt{Dt_1}}\right]\right)=0 \tag{2 7}$$

Eqn. (2.5) then can be rewritten as,

$$\frac{e^{-x^2/4Dt_2}}{2\sqrt{Dt_2}}=\frac{e^{-x^2/4Dt_1}}{2\sqrt{Dt_1}} \tag{2 8}$$

The solution of these equations can be found by taking the logarithm

$$-\left(\frac{x}{\sqrt{4Dt_2}}\right)^2-\ln\left(2\sqrt{Dt_2}\right)=-\left(\frac{x}{\sqrt{4Dt_1}}\right)^2-\ln\left(2\sqrt{Dt_1}\right) \tag{2.9}$$

Solving Eqn. (2.9) for x, one gets

$$x^2=\frac{2D\ln\left(t_2/t_1\right)}{(1/t_1)-(1/t_2)} \tag{2.10}$$

Hence, solutions of x giving the two extremes are

$$x_1=\sqrt{\frac{2D\ln\left(t_2/t_1\right)}{(1/t_1)-(1/t_2)}}\quad and\quad x_2=-\sqrt{\frac{2D\ln\left(t_2/t_1\right)}{(1/t_1)-(1/t_2)}} \tag{2.11}$$

Subtraction of x_1 from x_2 will give the separation between the two extremes d,

$$d=x_1-x_2=2\sqrt{\frac{2D\ln\left(t_2/t_1\right)}{(1/t_1)-(1/t_2)}} \tag{2.12}$$

Then the diffusion coefficient can be written as,

$$D=\frac{d^2\ [(1/t_1)-(1/t_2)]}{8\ln\left(t_2/t_1\right)} \tag{2.13}$$

Since the refractive index at different planes in the cell are different, the light passing through the cell will have different optical paths at different planes given by[4],

$$\Delta_1\left(x_1\right)=n_1\left(x_1\right)L,\ \ \Delta_2\left(x_2\right)=n_2\left(x_2\right)L,\ \ . . \tag{2.14}$$

where Δ_1, Δ_2, are the optical paths of the light rays through different planes situated at x_1, x_2, and n_1, n_2, are the corresponding refractive indices of the planes and L is the thickness of the cell (2 5 cm). The orientation of the experimental cell and change in the path length of the light traveling through the cell is shown in Fig. 2.5 for small t. It can be seen that the optical paths through different planes are different, producing a shift in the fringes with position as well as time (due to diffusion). Therefore by measuring the fringe shift with time, the diffusion coefficient can be found. It was found that in all the cases the difference between the extreme points were equal to the shift in the extreme points of the interferogram during the same time interval

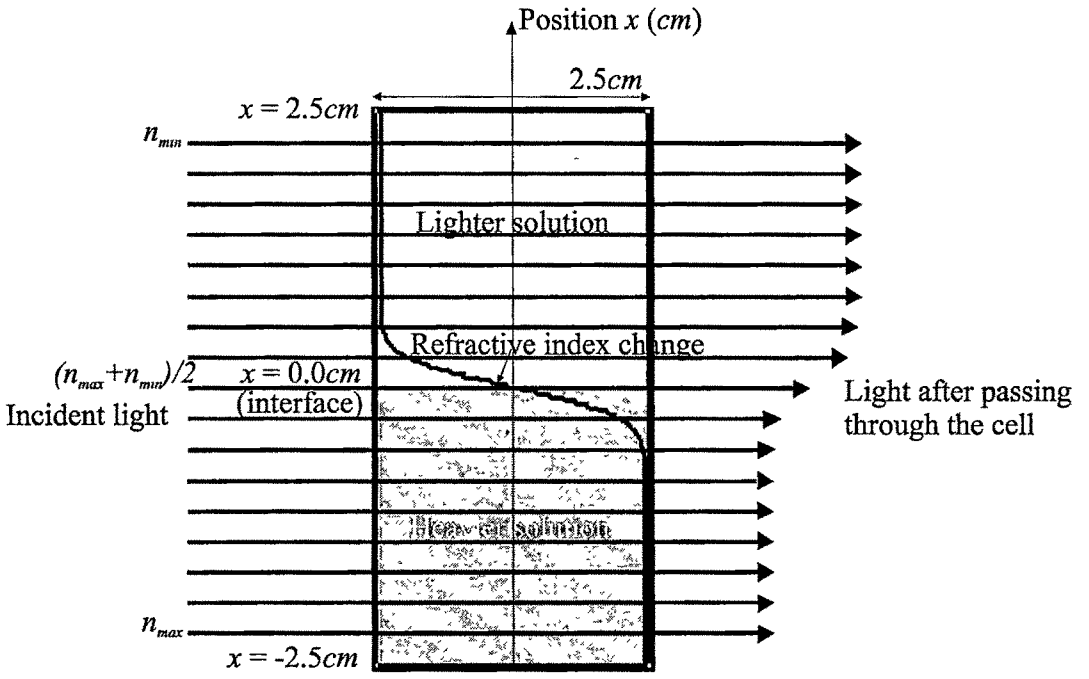

Figure 2.5: Change in the path of the incident beam inside the experimental cell

2.1.8 Diffusion Studies Using Michelson Interferometer

In this technique, conventional Michelson's Interferometer setup is used and is shown in Fig. 2 6[13]. The source used was a 30 mW He-Ne laser (632 8 nm) The laser beam is expanded using a spatial filtering assembly (SF) and split into two using a beam splitter (BS) The transmitted and the reflected beams fall on mirrors M_1 and M_2 respectively. The glass cell (G) containing the experimental solutions is placed in one of the arms of the interferometer (here in the reflected beam arm). After reflection from these mirrors and passing through the diffusing liquids, the beams interfere at the screen. The path difference between the rays from M_1 and M_2 are adjusted such that circular fringes are observed on the screen. The interference patterns are captured by a CCD (charged coupled device) camera and are stored in a PC. The CCD camera has 512×512 pixels (pixel of size $9.8\mu m \times 9\ 8\mu m$ and 8-bit dynamic range). These interference patterns are used for the calculation of diffusivity. The cell filling procedure is as explained in the previous section 2.1.6 The heavier solution introduced below will push the lighter solution to the top of the cell. The two solutions will form two different interference patterns at the detector plane (screen) as their

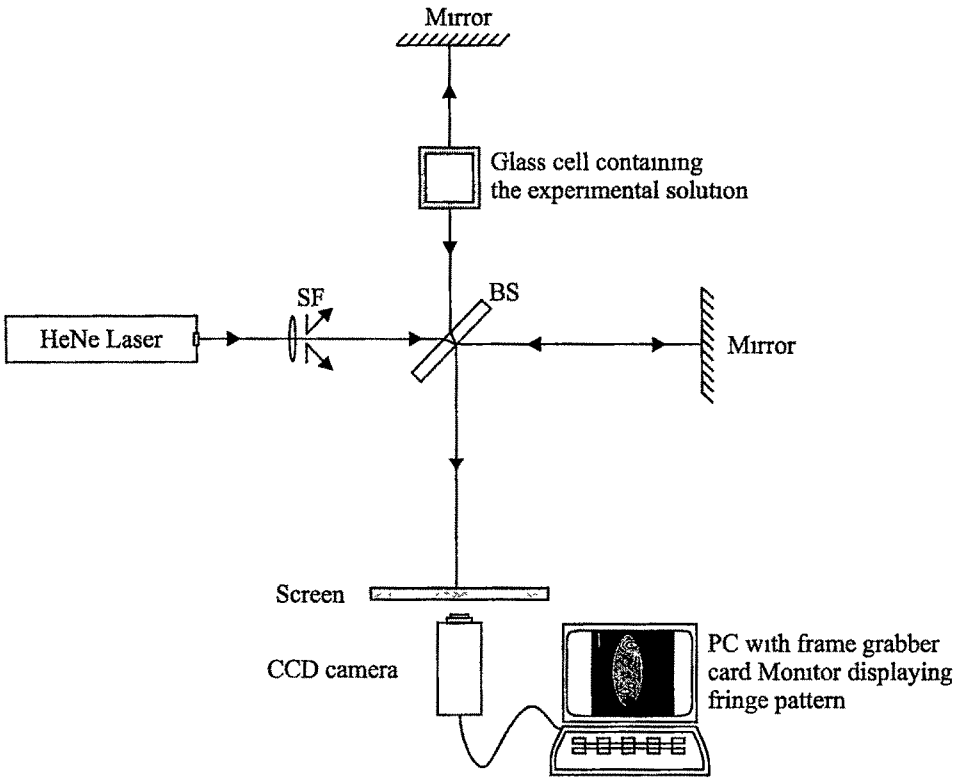

Figure 2.6: Michelson Interferometer Experimental Setup

refractive indices are different. The mirrors are adjusted after the introduction of the heavier solution to get the fringe pattern due to both the solutions. Formation of two distinct interference patterns can be understood from the plot between refractive index and diffusion direction for different instances of time shown in Fig 2.3. From the figure, it can be seen that beyond 1 cm from the interface, the refractive index remains constant even after 300 min of diffusion which means that the change in refractive index is sharp. The fringe pattern due to both the solutions will therefore coexist. Since the concentration and hence the refractive index at a particular plane changes with time, the fringe pattern will also shift with time. The shift of the fringes is equivalent to the shift in the extreme points x_1 and x_2. As the diffusion progresses with time the centers of the two fringe patterns due to both diffusing solutions, will shift outward. To calculate the diffusion coefficient, it is sufficient to measure the distance d between the centers of the two fringe patterns in the interferograms at times t_1 and t_2 and using it in Eqn. (2.13). The experiments were carried out at a temperature of 25 ^oC and interferograms are recorded via CCD camera in the PC

every 15 min.

Experimental Results and Discussion

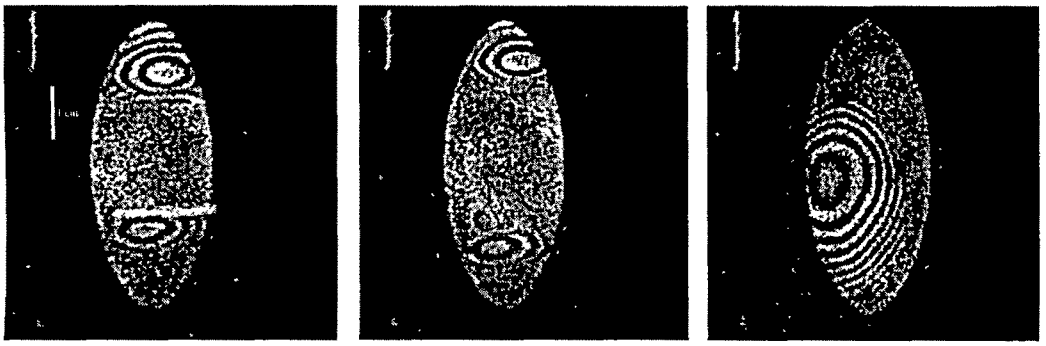

(a)after 30 min (b)after 90 min (c)at equilibrium

Figure 2.7: Change in fringe pattern with time for an average concentration of 0.4981 mol l^{-1} using Michelson Interferometer

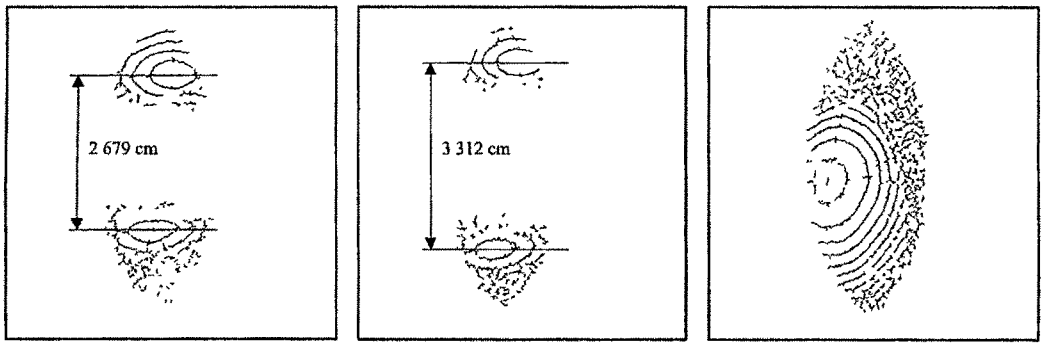

Figure 2.8: Traces of figures 2 7a, 2.7b and 2.7c respectively

Figures 2.7a to 2.7c show the interferograms for a solution of average concentra-tion 0 4981 mol l^{-1} at 30 min, 90 min and at equilibrium respectively. Fringe systems due to heavier and lighter solutions can be seen clearly in the figures The separation between the two extreme points d is found from the vertical shift in the fringe pattern for this (30 min – 90 min) time interval using the computer traces of the interferograms. The traces are made, by first converting the interferograms into binary images, and then using simultaneous vertical and horizontal scans[60, 61].

Computer trace of the interferogram makes the identification of fringes as well as measurement of the vertical shift easy. The traces for the interferograms in Figures

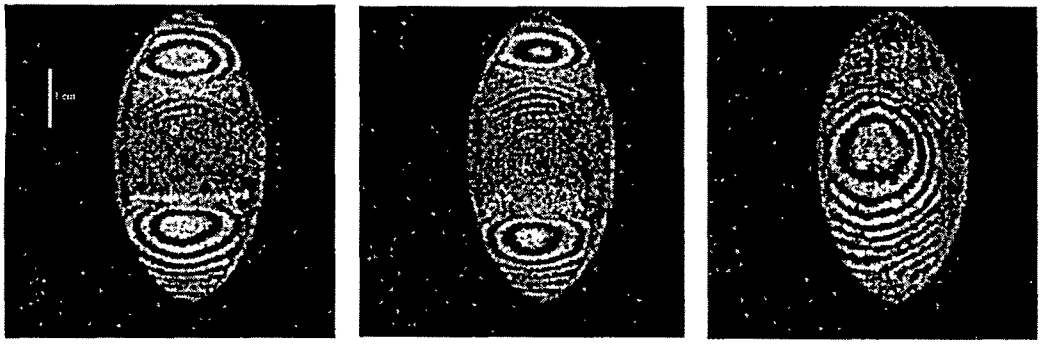

(a)after 30 min (b)after 90 min (c)at equilibrium

Figure 2 9: Change in fringe pattern with time for an average concentration of 1.9907 mol l^{-1} using Michelson Interferometer

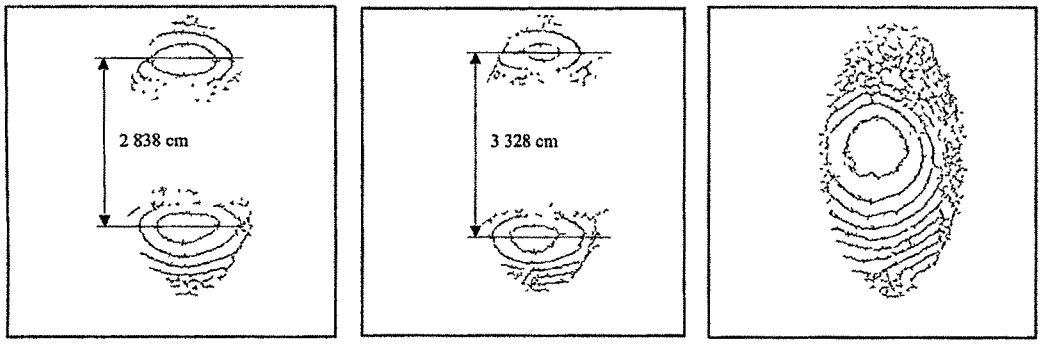

Figure 2.10: Traces of figures 2.9a, 2.9b and 2.9c respectively

2 7a to 2.7c are shown in Figures 2.8a to 2.8c respectively. The value of d for this time interval is found from the traces to be 0.453 cm. The corresponding diffusion coefficient is 8.65×10^{-6} cm^2/sec. Figures from 2.9a to 2.9c show the interferograms for an average concentration 1.9907 mol l^{-1} at 30 min, 150 min and at equilibrium respectively. The traces for these fringes are shown in Figures 2.10a to 2.10c respectively. The corresponding d is 0.40 cm and the diffusion coefficient is 5.52×10^{-6} cm^2/sec. Average value of diffusion coefficient (D_{avg}) for a particular C_{avg} is obtained by calculating the diffusion coefficients for different time intervals. The calculated diffusivity values (D_{avg}) for Ammonium dihydrogen phosphate for different concentrations at 25 ^oC are tabulated in Table II. From Fig 2.9 it can be seen that the shift in the fringe patterns is small even for large time intervals indicating that diffusion process at high concentration is slow compared to low concentration and from the calculated values it can be seen that the diffusivity decreases with concentration as expected

The advantage of this technique is the monitoring of the diffusion process in real time in a PC. A particular fringe pattern is a characteristic of a particular concentration. Thus the movement of fringe pattern with time is a measure of diffusion process. Also the movement of fringe patterns with time proves that it is a case of unsteady-state diffusion and diffusivity value decreases with increase in concentration and finding the shift in the fringe pattern is fairly easy from the computer traces.

2.1.9 Diffusion Studies Using Multiple Beam Interferometer

The second technique uses a multiple beam interferometric method and the corresponding experimental setup is shown in Fig 2.11[14]. The light source used in this experiment was a 10 mW He-Ne laser (632.8 nm, 2 mm dia). This beam was expanded using a spatial filtering assembly and is collimated using lens (L). The collimated light is then allowed to pass through the cell containing the diffusing solutions. The light after passing through the cell falls on the multiple beam interferometer, which is a glass plate of 3 mm thickness and kept at an angle θ with respect to its normal. After multiple reflections from the interferometer, the beam will interfere at the screen S to produce interferograms. A CCD camera placed behind the screen will capture the interferograms every 5 min and these are stored in the PC for analysis. The process of diffusion can be studied from several consecutive interferograms.

Experimental Results and Discussion

As the diffusion starts several interferograms are formed. Figures 2.12a to 2.12c show the interferograms for a solution of average concentration 0 4981mol l^{-1} at 51 min, 70 min and at equilibrium respectively. The initial images are not used in the calculations because reflection from the interface makes it difficult to determine the extreme points in the fringe pattern The separation between the extreme points can be easily calculated. Vertical lines are drawn on the fringe pattern on both the sides of the interface ($x = 0$). Connecting these lines with a slanted line yields the extreme points (Fig 2.12b). The diffusion coefficient can be calculated from the shift in the extreme points d for two different times. The change in separation between

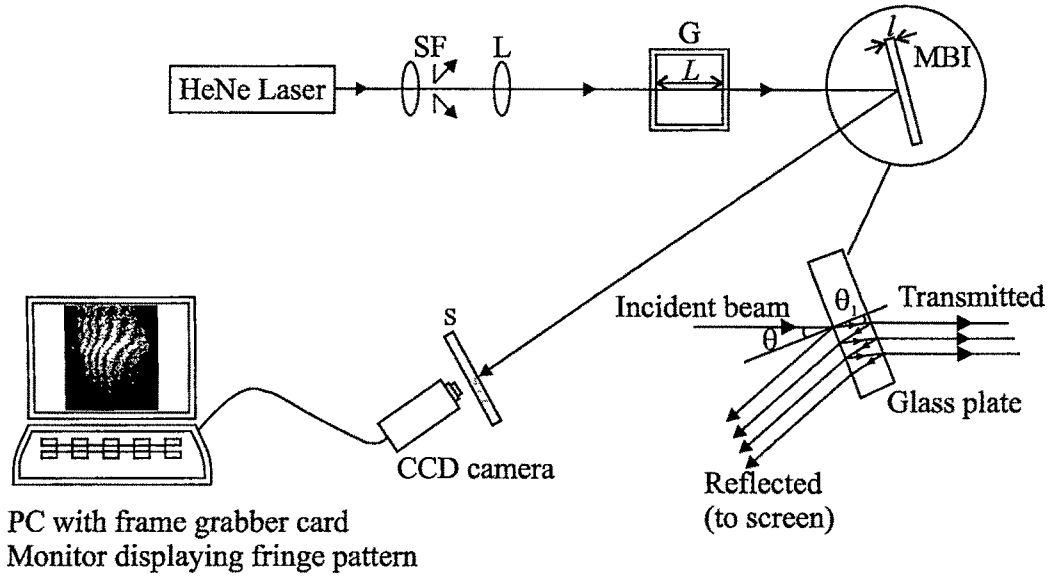

Figure 2.11· Experimental Setup

the extreme points d for the interferograms in Fig. 2.12a and 2.12b is 0.65 cm. The diffusion coefficient for this d value is 14.75 $\times$ 10^{-6} cm^2/sec at 35 ^oC (room temperature). Diffusion coefficient at 25 ^oC can be computed using the viscosity values and is equal to 8 55 $\times$ 10^{-6} cm^2/sec. The diffusion coefficients for different intervals of time are calculated and average diffusion coefficient is determined.

Figures 2.13a to 2.13c show the interferograms for a solution of average concentration 1 9907 mol l^{-1} at 51 mins, 70 mins and at equilibrium respectively. Here the interferometer and the collimating lens are adjusted so as to give thick interference fringes The value of d for this interval is 0.58 cm and the corresponding diffusion coefficient at 25 ^oC is 5.51 $\times$ 10^{-6} cm^2/sec. The values of average diffusion coefficients (D_{avg}) obtained for different average concentrations are tabulated in Table 2.2 along with the diffusion coefficient values from literature[19, 20]. As the concentration decreases, the diffusion coefficient increases and the progress of diffusion process becomes fast. This can be seen from the two sets of interferograms in Fig 2.12 and 2.13. The average concentration for the interferograms in Fig. 2.12 is less than that in Fig 2.13. So the separation between the extreme points is more in the case of Fig. 2.12 than Fig. 2.13 for the same time interval and the separation changes more quickly for a solution of lower concentration. The interferograms in this method should reflect the

change in refractive index (Fig. 2.1). As the diffusion progresses, the bends in the fringe pattern should also shift with time. At equilibrium, one should obtain straight line fringes

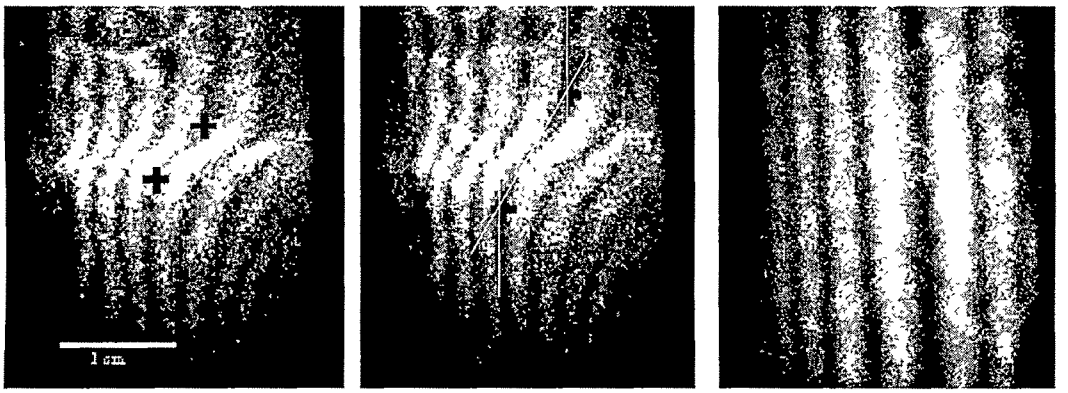

(a) after 51 min (b) after 70 min (c) at equilibrium

Figure 2 12: Change in fringe pattern with time for an average concentration of 0.4981 gmol l^{-1} using Multiple Beam Interferometer

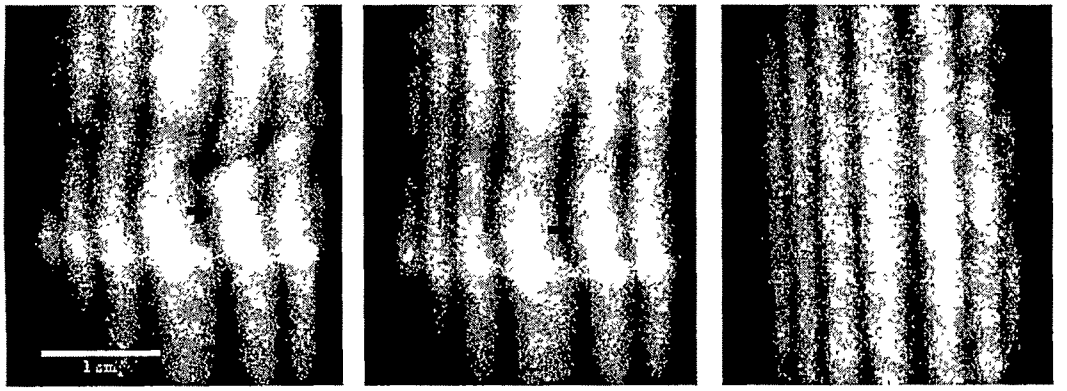

(a) after 51 min (b) after 70 min (c) at equilibrium

Figure 2.13. Change in fringe pattern with time for an average concentration of 1 9907 gmol l^{-1} using Multiple Beam Interferometer

This method does not require the strict optical arrangements unlike other methods and is less sensitive to external disturbances. The method is easy and cost effective. Low power diode lasers can also be used as the source. As the fringe pattern is characteristic of the diffusing solutions, by monitoring the change in the fringe pattern one can study the process of mass transfer using this method

2.1.10 Diffusion Studies Using White Light and artificially generated fringes

In this section a non-interferometric technique to measure diffusion coefficients of transparent binary liquid solutions using white light source is described[12, 15, 16]. Light rays passing through a non-uniform refractive index medium bend towards regions of higher refractive index[56]. The amount of the ray bending at various instances of time will depend upon the refractive index gradient existing inside the medium and hence on the diffusion coefficient. Therefore by measuring the bending of the ray the diffusion coefficient can be determined. This is achieved by using a fringe pattern at the entrance face of the diffusion cell. This fringe pattern was a series of black and white stripes at an angle with the horizontal, printed on a normal white paper using a laser printer. The fringe pattern is proportional to the bending of the light ray. The shift of the fringe pattern at different times is captured by a CCD camera and frame grabber card and is stored in a PC. Simple image processing of these stored images will yield the diffusion coefficient.

The experimental setup used is shown in Fig. 2.14 Light from the point white source (S) (6W) was allowed to fall of the fringe pattern. The fringe pattern was regularly spaced black and white bands subtending an angle of 50^{o} to the horizontal. The light then passes through the diffusion cell Half the volume of the cell is first filled by the solution of lower concentration. The heavier concentration solution of equal volume is introduced, below the lower concentration solution using a capillary tube mechanism. The fringe pattern is captured every minute by a CCD camera and frame grabber card and is stored in a PC for analysis. After the cell is filled, the diffusion process starts. Theoretical explanation of the method can be given by considering the medium as consisting of layers with different refractive indices resulting in a bending of the incident light beam[56]. The refractive index of each layer changes with time due to the diffusion process thereby changing the angle of bending. Hence a fringe pattern placed at the entrance face of the diffusion cell viewed at the exit face will have a shift from its equilibrium position (when the refractive index is uniform).

One can analyze this process theoretically using solution of the Fick's second law

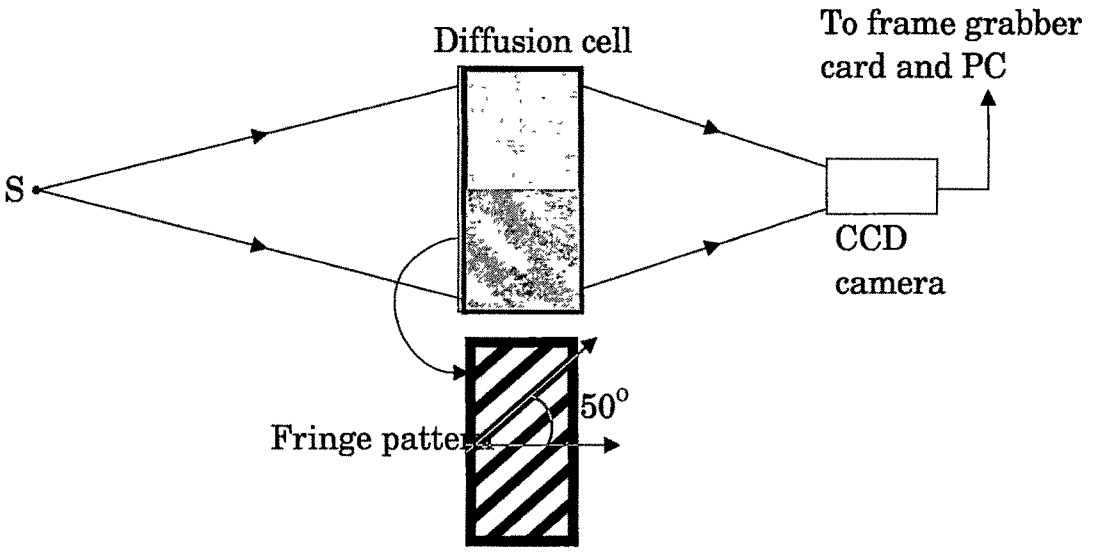

Figure 2 14: Experimental Setup

given by Eqn. (2.1) which governs free diffusion process in a binary liquid system consisting of liquids having concentrations C_1 and C_2, separated at $x = 0$ when $t = 0$. Considering diffusion along only one direction (x-axis) is given by Eqn.(2.2).

For the narrow range of concentrations over which the experiments were conducted, the refractive index inside the experimental cell can be considered as a linear function of concentration and is given by Eqn. (2.4).

As the diffusion process progresses the concentration gradient and hence the refractive index changes. The refractive index variation Δn as a function of x between times t_1 and t_2 ($t_2 > t_1$) is given by Eqn. (2.5).

The refractive index distribution inside the diffusion cell is non-uniform (Eqn. 2.4) resulting in the bending of light rays entering the cell. The amount of bending will depend on the refractive index gradient[38, 50, 57]. The change in position of the ray inside the cell due to bending is given by[56]

$$\frac{d}{ds}\left(n\frac{d\vec{r}}{ds}\right) = \vec{\nabla} \cdot n \tag{2.15}$$

Where s is the path length of the ray and is the position vector of a point on the ray. For one dimensional diffusion along x direction as shown in Fig. 2.15, the ray can be considered parallel to z axis. In this case, for a ray entering the cell at position x

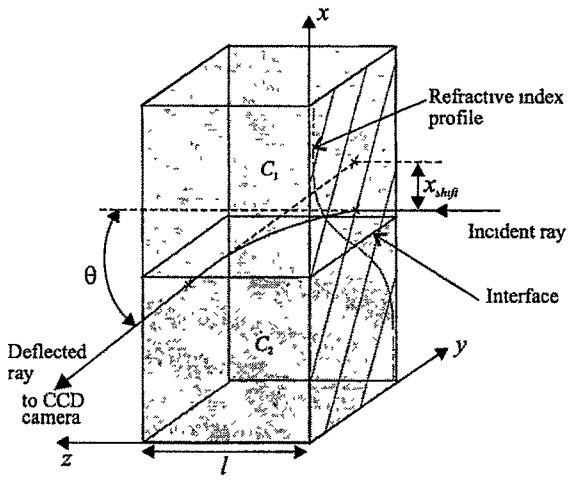

Figure 2.15: Beam deflection and resulting fringe shift

and considering the bending to be small (i.e. $ds \approx dz$) Eqn. (2.15) can be modified to[38, 57]

$$\frac{d}{dz}\left[n(x,t)\,\frac{dx}{dz}\right] = \frac{\partial n(x,t)}{\partial x} \tag{2.16}$$

For a ray entering the cell at $z = 0$ and position x, Eqn. (2.16) can be integrated with respect to z, to give the angle of bending. It is given by[43, 44]

$$\begin{aligned}\theta(x,t) &= \frac{dx}{dz} = \frac{1}{n}\int_0^l \frac{\partial n(x,t)}{\partial x}dz = \frac{l}{n}\,\frac{\partial n(x,t)}{\partial x} \\ &= \frac{l}{n}\left(\frac{dn}{dC}\right)_0\left(\frac{C_1 - C_2}{2}\right)\frac{\exp\left(-x^2/4Dt\right)}{\sqrt{\pi Dt}}\end{aligned} \tag{2.17}$$

where l is the length of the diffusion cell. The change in bending angle along the diffusion direction for different times is shown in Fig 2.16 (average concentration $C_{avg} = 0.9959$ mol l^{-1} of ammonium dihydrogen phosphate). It can be seen that the maximum bending occurs at the interface. As the time progresses the angle of bending also decreases (MATLAB code for bending angle with cell position is given in Appendix B.3). The change in the angle of bending can be assumed to be a constant in the time interval between t_1 and t_2 for a ray entering the medium at x for two different times t_1 and t_2 considering small concentration gradients, so that the refractive index n. It is given by

$$\delta\theta(x,t_1,t_2) = \theta(x,t_2) - \theta(x,t_1)$$

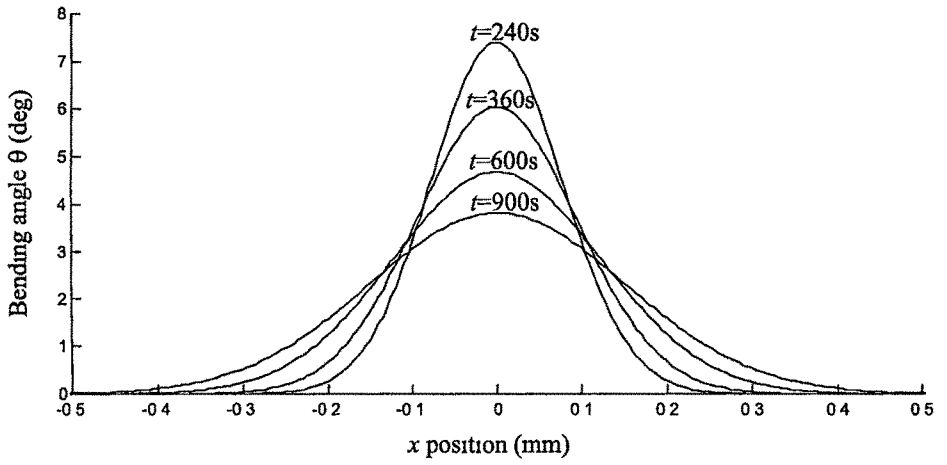

Figure 2 16: Change in deflection angle with diffusion direction at different instances of time

$$= \frac{l}{n}\left(\frac{dn}{dC}\right)_0\left(\frac{C_1 - C_2}{2}\right) \times \left[\frac{\exp\left(-x^2/4Dt_2\right)}{\sqrt{\pi D t_2}} - \frac{\exp\left(-x^2/4Dt_1\right)}{\sqrt{\pi D t_1}}\right] \quad (2.18)$$

The graphical representation of Eqn. (2.18) is shown in Fig 2 17 (average concentration $C_{avg} = 0.9959$ mol l^{-1}). It can be seen that this curve has three extremes. These extremes can be found by differentiating Eqn. (2.18) and equating to zero

$$\frac{d}{dx}\left[\delta\theta\left(x, t_1, t_2\right)\right] = \frac{l}{n}\left(\frac{dn}{dC}\right)_0\left(\frac{C_1 - C_2}{2}\right) \times \left[\frac{x\ \exp\left(-x^2/4Dt_1\right)}{2\,D\,t_1\sqrt{\pi D t_1}} - \frac{x\ \exp\left(-x^2/4Dt_2\right)}{2\,D\,t_2\sqrt{\pi D t_2}}\right] = 0 \quad (2.19)$$

Therefore

$$\frac{x\ \exp\left(-x^2/4Dt_2\right)}{2\,D\,t_2\sqrt{D t_2}} = \frac{x\ \exp\left(-x^2/4Dt_1\right)}{2\,D\,t_1\sqrt{D t_1}} \quad (2.20)$$

One of the solutions of Eqn. (2.20) is $x = 0$, the interface. The other two solutions can be found by taking logarithm of the equation. This leads to

$$x^2 = \frac{4\,D\,\ln\left(t_1^{3/2}/t_2^{3/2}\right)}{(1/t_2) - (1/t_1)} \quad (2.21)$$

The two solutions are

$$x_1 = \left[\frac{4\,D\,\ln\left(t_1^{3/2}/t_2^{3/2}\right)}{(1/t_2) - (1/t_1)}\right]^{1/2} \quad (2\ 22)$$

and

$$x_2 = -\left[\frac{4\,D\,\ln\left(t_1^{3/2}/t_2^{3/2}\right)}{(1/t_2) - (1/t_1)}\right]^{1/2} \quad (2.23)$$

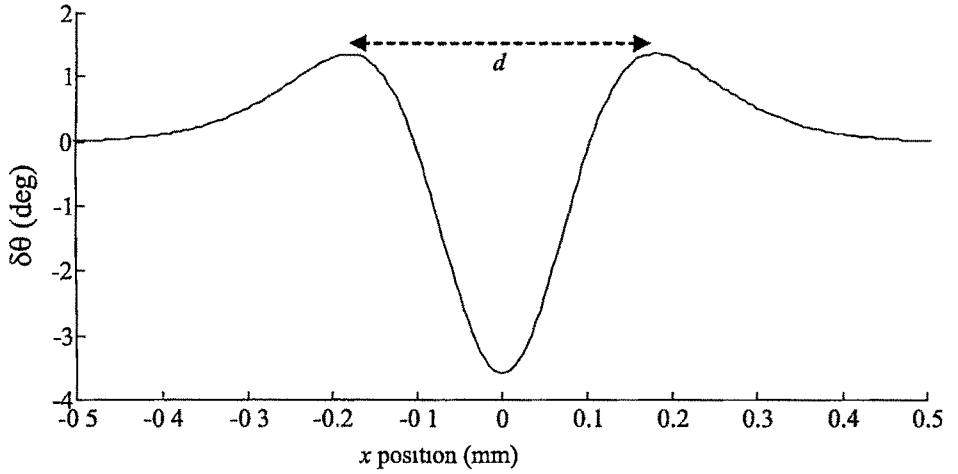

Figure 2.17. Change in Change in $\delta\theta$ with diffusion direction ($t_1 = 240s,\ t_2 = 900s$)

Subtracting Eqn. (2.23) from Eqn. (2.22) and taking square yields the diffusion coefficient D. It is given by

$$D = \frac{d^2\left[(1/t_2) - (1/t_1)\right]}{16\ln\left(t_1^{3/2}/t_2^{3/2}\right)} \tag{2.24}$$

where $d = x_1 - x_2$ is the separation between the two extremes. From Fig. 2 15 and Eqn. (2.17) it can be seen that concentration gradient will lead to a non-uniform refractive index distribution inside the cell resulting in bending of the incident light rays. This will reflect as a shift in the fringe pattern from its equilibrium position and is proportional to the bending angle (Fig. 2.16) and hence the refractive index. The local fringe shift x_{shift} is given by

$$x_{shift}(x,t) = l\ \tan\left[\theta(x,t)\right] \tag{2 25}$$

The difference in fringe shift with diffusion direction for two instances of time t_1 and t_2 is

$$\begin{aligned} \delta x_{shift}(x,t_1,t_2) &= x_{shift}(x,t_2) - x_{shift}(x,t_1) \\ &= l\ \{\tan\left[\theta(x,t_2)\right] - \tan\left[\theta(x,t_1)\right]\} \\ &= l\,\delta\theta(x,t_1,t_2) \end{aligned} \tag{2.26}$$

In Eqn. (2.26) it is assumed that the angle of bending is small so that $\tan\theta \simeq \theta$. From Eqn. (2.26), it can be seen that the difference in fringe shift is proportional to

the difference in bending angle. The difference of the fringe shifts at two instances of time will give a plot similar to Fig. 2.17 with three characteristic extremes, which depends on the diffusion coefficient of the binary liquid solution. By substituting the difference between the extremes of this plot in Eqn. (2.24) the diffusion coefficient can be calculated.

Experimental Results and Discussion

From Fig. 2.16 it can be seen that the change in angle of bending of the incident ray is large at the initial stages of diffusion. Here the fringe shifts (x_{shift}) and hence the difference between the fringe shifts (δx_{shift}) will be appreciable Therefore the measurements use fringe shifts for $t < 3600s$. The experimental solutions are prepared by dissolving Ammonium dihydrogen phosphate in distilled water. The fringe patterns are recorded in the PC via CCD camera every 60 sec.

Fig. 2.18a to 2.18c shows the temporal evolution of the fringe pattern for a solution of average concentration 0 9958 mol l^{-1}. It can be seen that the fringe shift decreases with time. This is in accordance with Eqn. (2.17). The fringe patterns are traced by thresholding the image with the average gray value and simultaneous row and column scan[60]. These traces are shown in Fig. 2.19. The diffusion coefficients are calculated using the different fringes, for different time intervals and an average is found. The fringes used for the determination of diffusion coefficients are marked in the figure. The difference pattern obtained for the fringe marked as 1 in Fig. 2.19a and 2 19b is shown in Fig. 2.20. The separation d is obtained from least square fit of the experimental data. The solid line represents the fitting curve. A code written using MATLAB is used to trace the fringes, get the fringe shifts, fit the experimental data and to get the separation $d = 0.362$ cm. The calculated diffusivity value at 25 ^{o}C for the fringe shift shown in Fig. 2.19 is $7.28 \times 10^{-6}\ cm^2/s$.

Fig. 2.21a to 2.21c shows the temporal evolution of the fringe pattern for the solution of concentration 1.9907 mol l^{-1}. The traces for this fringe patterns are shown in Fig. 2.22. The fringes used for the determination of diffusion coefficients are marked. The x_{shift} for the fringe marked 1 in the Fig 2.22 is shown in Fig. 2.23. The obtained

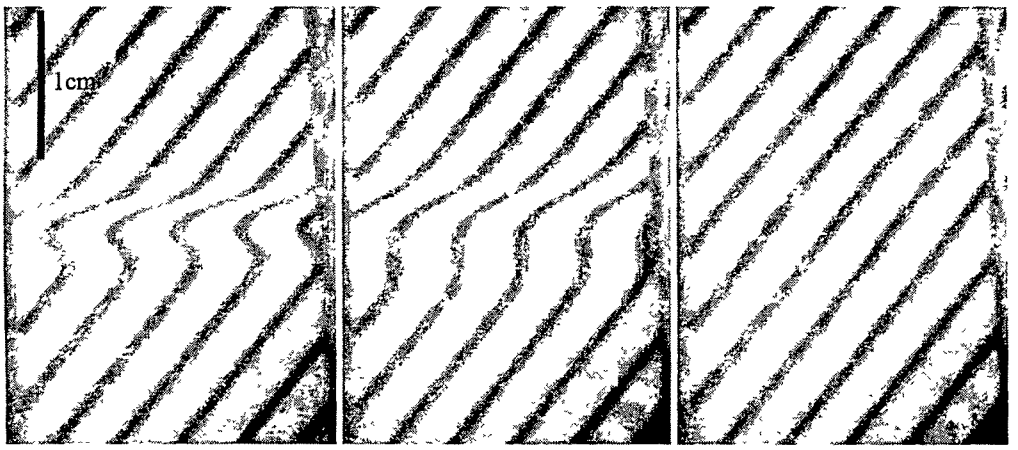

(a) after 240sec (b) after 900sec (c) at equilibrium

Figure 2.18: Change in fringe pattern with time for average concentration C_{avg} = 0.9959 mol l^{-1}

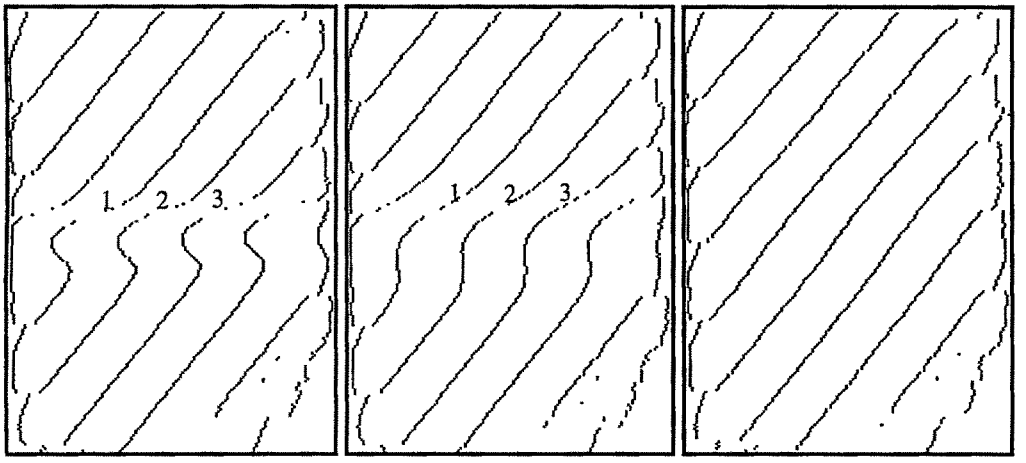

Figure 2 19: Trace of Figures 2.18a, 2.18b and 2.18c respectively

d from the least square fit of this plot is 0 319 cm and the corresponding diffusion coefficient at 25 ^{o}C is 5.69×10^{-6} cm^2/s.

The experiment is repeated using solutions of different concentrations. The obtained average diffusion coefficients are given in Table 2.2, along with the reported literature values[19], using Gouy interferometry which is considered to be one of the most precise method to measure diffusion coefficients

The main advantageous feature of this technique is non-interferometric nature and

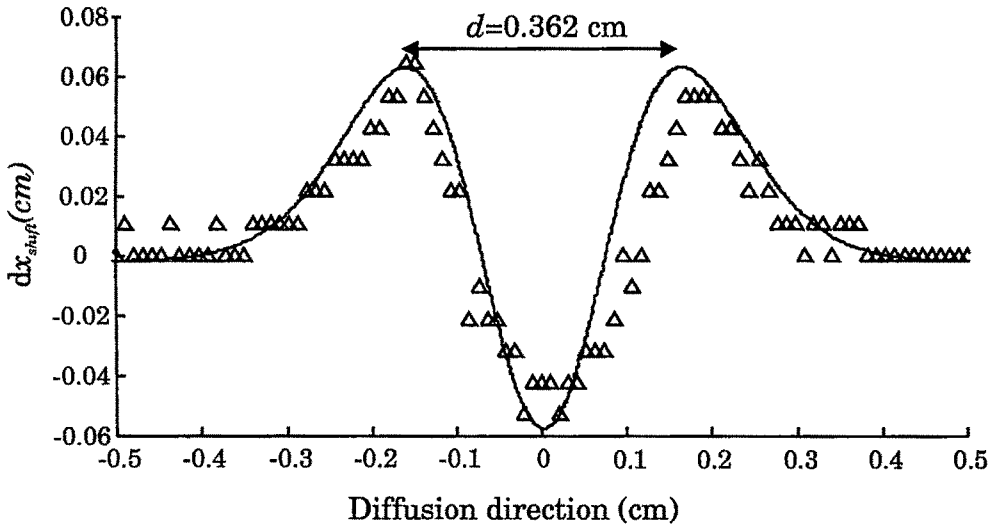

Figure 2.20. Plot of change in fringe shift (δx_{shift}) with diffusion direction for average concentration $C_{avg} = 0.9959$ mol l^{-1} ($t_1 = 240$ s, t_2 900 s)

therefore it does not require the stringent optical conditions of interferometric methods making it cheap and easy to implement. This technique can be implemented in any environment with limited optical requirements and is found to be less sensitive to external disturbances. The processing of the fringe patterns is also easy and accurate diffusivity measurements are possible. In this technique the process of diffusion can be investigated in real time as the fringe shift with time, which is the representative of diffusion, is obtained in the PC in real time.

On the negative side, it is found that the concentration difference between the diffusing solutions should be larger in this technique with compared to that in interferometric technique. This may affect the assumption that the diffusion coefficient is a constant between the concentration ranges of the diffusing solutions. But the experimental results show that it does not affect the obtained diffusivity values, which are comparable with other methods This validates the theory described.

The resolution of the measurement of separation d is increased by fitting the experimental data. Even without the fit, the results are found to be accurate. The resolution can be further increased by keeping the CCD camera closer to the experimental cell so that only the portion near the interface is imaged.

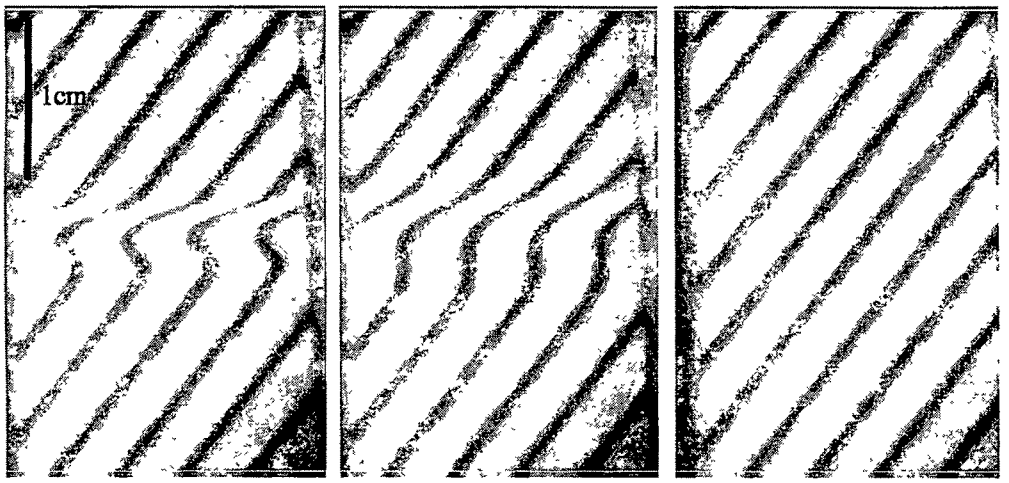

Figure 2.21: Change in fringe pattern with time for average concentration C_{avg} =1.9907 mol l^{-1}

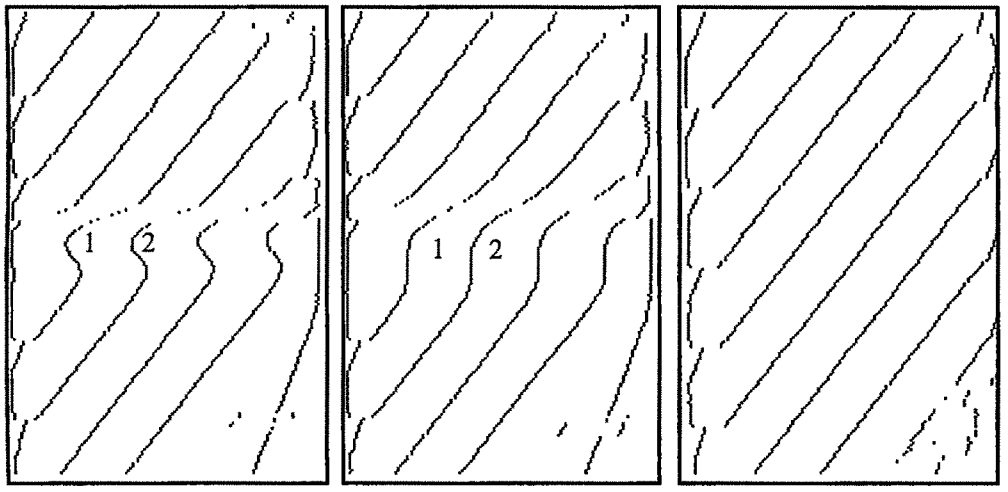

Figure 2.22: Trace of Figures 2.21a, 2.21b and 2.21c respectively

2.1.11 Conclusion

Three new optical methods to measure unsteady state diffusion coefficients of binary liquid solutions are developed. All the developed methods yield accurate diffusion coefficients. The obtained diffusion coefficients for various concentrations are tabulated in Table 2.2 along with the diffusion coefficients from the literature.

The error in the calculated diffusion coefficient is shown in Fig. 2.24. It can be seen

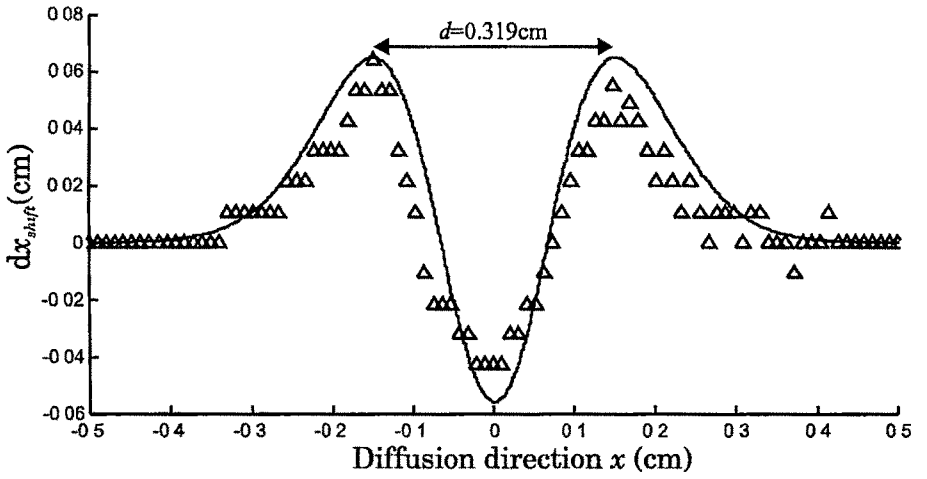

Figure 2.23: Plot of change in fringe shift (δx_{shift}) with diffusion direction for average concentration C_{avg} = 1 9907mol l^{-1} (t_1 = 240 s, t_2 = 900 s)

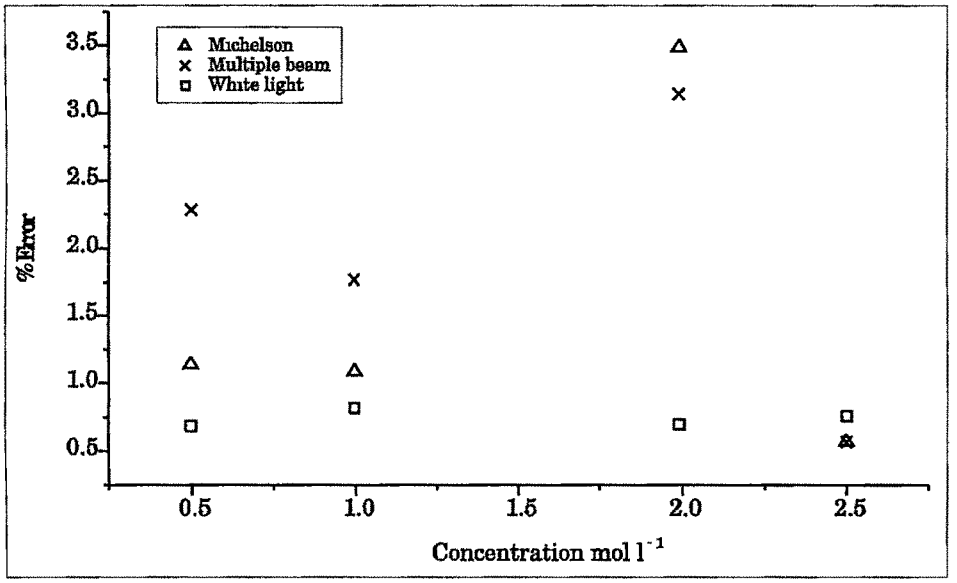

Figure 2.24: Variation of percentage error in calculated diffusion coefficients with concentration

that in all the cases the error is < 4%. The error in measurement is least in the method using white light and artificial fringes (< 2%). This is because a least square fitting is employed to determine the distance between the extreme points. In all the developed methods the extreme points can be found out fairly easily.

The concentration difference between the diffusing solutions in Michelson interferometric technique and multiple beam technique are small. In the method using artifi-

Table 2.2: Calculated diffusion coefficients

Concentration mol l^{-1}	Diffusion coefficient $D_{avg} \times 10^6$ cm^2/s at 25^oC				
	Michelson	Multiple beam	White light	Hatfield et al	Mullin & Cook
0.4981	8.65	8 55	8.81	8.75	8.5
0.9959	7.27	7.22	7.29	7.35	7.3
1.9907	5 53	5.55	5.69	5.73	5.3
2.4988	5.25	5.31	5.20	5.28	4.4

cial fringes and white light, the concentration difference employed should be larger. But this does not affect the theory developed to describe this method as can be seen from the results. This method is the easiest of the three developed methods for data acquisition and analysis. But the other two methods are also fairly easy to implement. The methods are less sensitive to external disturbances with the exception of Michelson interferometer technique, where care should be taken to reduce the external disturbances The methods are also easy to construct and are cost effective and can be implemented in any environment.

Automatic fringe tracing and extreme point measurement has been employed for the white light method making the measurement of the diffusion coefficient totally free from manual operations As all the developed methods are monitored in real-time, they yield valuable information about the diffusion process. Any disturbance in the diffusion cell will reflect as a change in the fringe system and can be monitored in real-time. Table 2.3 shows a comparative study of some of the methods used for measuring diffusion coefficients[50].

Table 2.3: Comparative study of methods used to measure diffusion coefficient

Method	Nature of diffusion	Expense	Apparatus construction	Conc. difference	Accuracy (%)
Diaphragm cell	Pseudosteady state	Small	Easy	Large	0.2
Taylor dispersion	Decay of a pulse	Moderate	Easy	Average	1
Gouy interferometer	Unsteady state	Large	Moderate	Small	<0.1
Rayleigh interferometer	Unsteady state	Large	Difficult	Small	0.2
Holographic interferometry	Unsteady state	Moderate large	Difficult	Small	<1
ESPI	Unsteady state	Moderate	Moderate	Small	1
Speckle decorrelation	Unsteady state	Small	Very easy	Small	5
Digital moiré	Unsteady state	Small moderate	Easy	Small	1
Michelson Interferometer	Unsteady state	Moderate	Easy	Small	<4
Multiple beam interferometer	Unsteady state	Small	Easy	Small	<4
White light	Unsteady state	Small	Very easy	Average	<2

2.2 Hairiness measurement of textile yarns using crossed polarizers

Textile yarn is made up of many fibers. But some of the fibers protrude out from the yarn body. These fibers constitute the hairiness of the textile yarn. For the textile industry, the comfort properties of the fabrics is a very important issue. The tactile feel and the look of the fabric are affected by this hairiness Hair lengths vary from less than 0.1 mm to several millimeters. Even hairs of length shorter than 0.1 mm can be significant for touch. Hence most of the times yarn hairiness is an undesirable property which has to be measured and controlled.

Over the years, many researchers have developed techniques for yarn hairiness studies. Most of the developed techniques for hairiness measurement are optical methods or optical and photoelectric methods applied simultaneously[21]. Many of the developed optical methods are approximate and require very sensitive measuring equipments. So development of new easy to implement, fast and cost effective methods to measure the hairiness becomes necessary.

In this section a very simple and sensitive method developed to measure hairiness of textile yarns from the light scattered by the protruding hair fibers using a pair of crossed polarizers is discussed. It was found that the amount of light scattered by the textile yarn increases linearly with hairiness. A linear fit to the hairiness-scattered light intensity plot can be used to find unknown hairiness. The error of the method is calculated for different hairiness regions. It is found that when the hairiness is high the error of the method is as low as 1%. The method is also found to be very sensitive. With proper calibration, this method can be used to measure hairiness very accurately.

2.2.1 Hairiness

As mentioned in the previous section, the hairiness in textile yarns is caused by the fibers, which are not contained in the yarn body. Figures 2.25 and 2.26 show the yarn

profile parallel and perpendicular to the yarn axis respectively [21]. Fig. 2.27 shows the photograph of the yarn profile parallel to yarn axis[62].

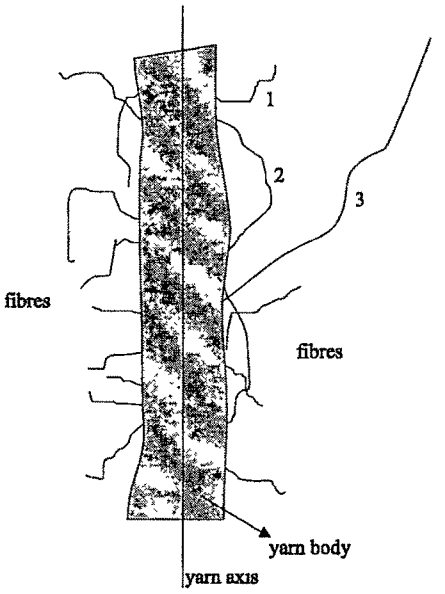

Figure 2.25: Yarn profile parallel to yarn axis

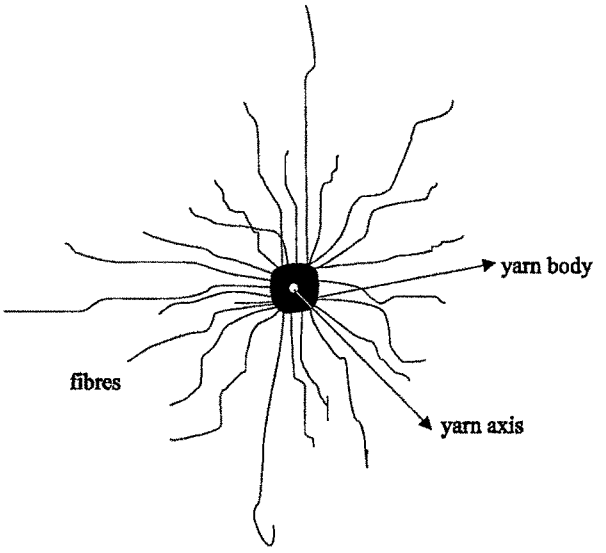

Figure 2.26: Yarn profile perpendicular to yarn axis

From Figures 2.25 to 2 27 it can be seen that the hairiness is formed by 1) the protruding fiber ends, 2) the looped fibers arched out of the yarn core and 3) the wild fibers. Fig 2.26 shows the profile of the yarn perpendicular to the yarn axis. But practically this sort of projection is difficult to obtain. Most of the optical techniques

Figure 2.27· Photograph of profile parallel to yarn axis[62]

use the projection of yarn profile onto a plane parallel to the yarn axis[21] In the method discussed here the scattering of light of a yarn profile parallel to the yarn axis is used for hairiness measurement[63]. The usual hairiness measurement parameters based on optical methods are as follows[21]

N_1 = number of protruding fibers per unit length of the yarn
N_2 = number of fiber loops per unit length of the yarn
N_3 = number of wild fibers per unit length of the yarn
N_y = number of protruding ends at a distance y from the axis of the yarn
L_1 = mean fiber length (in mm) of the protruding fiber ends
L_2 = mean fiber length (in mm) of the protruding fiber loops
L_3 = mean fiber length (in mm) of wild fibers
L_f = mean fiber length (in mm) of the fibers extracted from the core
L_1' = mean fiber length of the protruding hairs in the radial direction of the yarn

For the method discussed here, the hairiness length can be given by the following parameter

$$H = L_1 + L_2 + L_3 \tag{2.27}$$

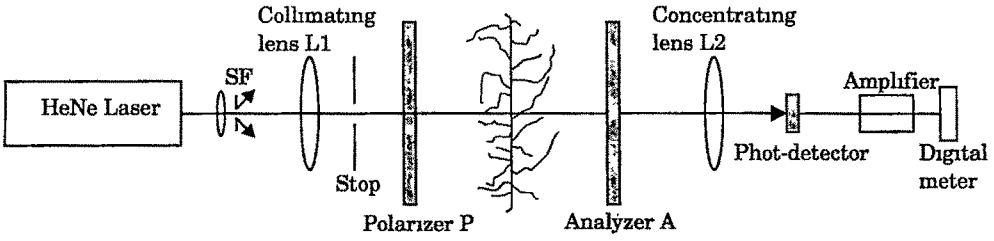

Figure 2.28: Experimental setup for measuring hairiness

Where H is the hairiness index, which is the total length of the protruding fibers per unit length the yarn (therefore unit less). L_1, L_2 and L_3 are as explained above. Therefore the measure of hairiness will be the total length of all the fibers protruding from the yarn per unit length of the yarn (1 cm).

2.2.2 Experimental setup and theory

The experimental setup for measurement of hairiness is shown in Fig. 2.28. Light form a He-Ne laser (10mW, 632.8nm) source is expanded using a spatial filtering assembly SF and collimated using lens L_1. The beam size is reduced to 1 cm using a rectangular stop. This beam size is reduced to this value because in textile industry usually the hairiness is measured as the total length of the protruding fibers per centimeter of the textile yarn. This beam is then polarized using a linear polarizer P. The collimated light is then allowed to fall on the textile yarn under test. The light after falling on the yarn will pass through an analyzer A, which is also a linear polarizer, with its plane of polarization perpendicular to that of the polarizer. A lens L_2 is used to concentrate the output from the analyzer towards a photodiode. The signal from the photodiode was amplified using a current-voltage converter and was measured using a sensitive digital meter. The amount of light reaching the photodiode is given by Malu's law[5]

$$I = I_0 \cos^2 \theta \tag{2.28}$$

where I is the output intensity from the analyzer, I_0 is the incident intensity on the analyzer and θ is the angle between the plane of polarization of the incident light and analyzer (A). From Eqn. (2.28) it can be seen that when the two polarizers are crossed (plane of polarization perpendicular, $\theta = 90^o$), then there will not be

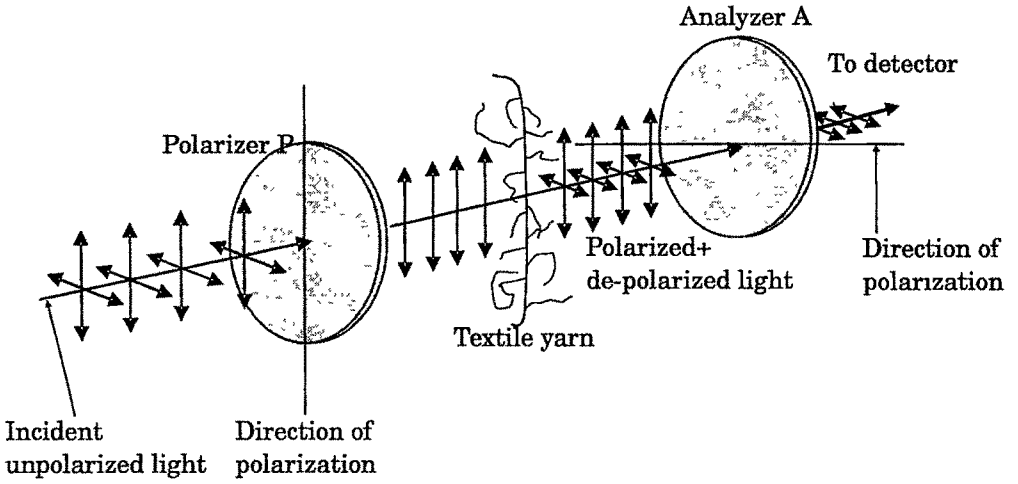

Figure 2.29: De-polarization of incident polarized light due to scattering

any output from the analyzer, when there is no yarn present in the setup. When yarn is introduced in the setup after the polarizer, some portion of the polarized light gets scattered from the hair fibers due to diffraction, refraction as well as reflection, making a portion of the incident plane polarized light de-polarized. This process is shown schematically in Fig. 2.29. This de-polarized light will have a component along the direction of polarization of the analyzer, resulting in a finite output from it.

The output from the analyzer depends upon the scattering of the light from the yarn hairs. More the hairiness greater will be the amount of scattered light and hence more will be the output from the analyzer. Therefore yarns having different hairiness will produce different outputs. The scattering from the hairs can therefore be used as the parameter to measure the hairiness. Some of the marketed instruments use the detection of scattered light from the fibers on the yarn body to measure hairiness[21, 64, 65]. But in these methods, a stop is necessary to filter out the direct beam (un-scattered) falling on the photodiode. This will introduce some errors as there could be scattering along the propagation direction of the direct light also, containing information about hairiness. But in the present method, all the hairiness information is passed on to the photo-detector, because the polarized direct beam will be stopped by the analyzer while the scattered light due to yarn hairiness will be passed on to the detector. The analyzer will act as a filter, passing only the hairiness information. This makes the technique quite sensitive and accurate

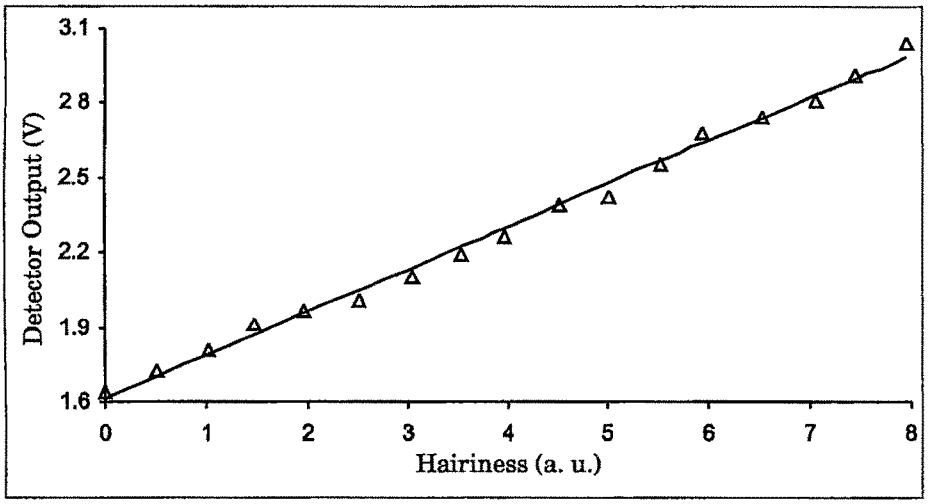

Figure 2.30. Variation in detector output with hairiness (calibration plot)

2.2.3 Results and discussion

The setup is first calibrated using yarns having known hairiness. The hairiness of the yarn is first measured by projecting its image onto a screen and measuring the total hair length. Section of the yarn without any protruding hairs is first introduced. This produces a finite output at the detector. This output is due to the scattering from the yarn body alone. The size of the yarn body is assumed to be a constant. This assumption may introduce some errors in the measured hairiness. Using yarns having known hairiness, the output from the analyzer is measured. The variation of the detector signal with hairiness is shown in Fig. 2.30. This figure represents the average of several measurements From the figure, it can be seen that the variation is almost linear over the whole range of hairiness A linear fit to the plot is found. The straight line in Fig. 2.30 is a linear fit. This linear fit is used to find unknown hairiness. The calculated values along with the hairiness measured from projection are given in Table 2.4 (the table also gives the percentage deviation of the linear fit from the values measured using projection) Unknown yarn hairiness was measured from output of the analyzer using the calibration plot (linear fit). The error in the method for different hairiness regions is calculated with yarns having unknown hairiness (the hairiness is later measured using projection method) and is plotted in Fig 2.31. From Fig. 2.31 it can be seen that the error increases with decrease in hairiness.

Table 2.4: Measured hairiness form scattered light and projection

Hairiness from projection (a. u.)	Detector output (V)	Detector output using Linear fit (V)	% deviation of linear fit
0 00 (no hairiness)	1.643	1.618	1.55
0.52	1 728	1.707	1.20
1.02	1.809	1.794	0.86
1.48	1 912	1.873	2.10
1.97	1.968	1.957	0.56
2.51	2.012	2.050	1.85
3.04	2.109	2.141	1.51
3.53	2.191	2.226	1.56
3.97	2 269	2.301	1.41
4.52	2.391	2.396	0 21
5.01	2.428	2.480	2.11
5.53	2.551	2.570	0.74
5.94	2.682	2.641	1.57
6.52	2.749	2.740	0.32
7.06	2 812	2.833	0.75
7 44	2.917	2.899	0.63
7.97	3.045	2.990	1.84

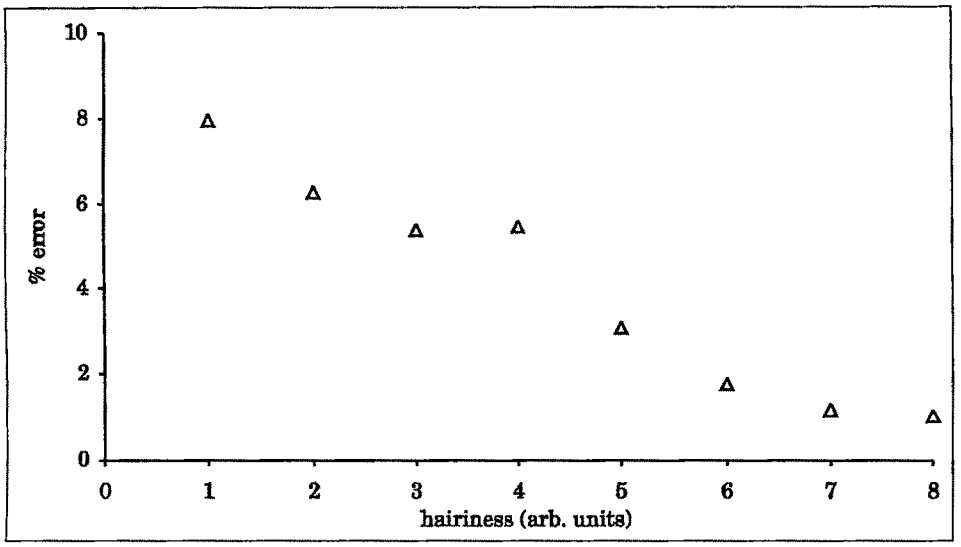

Figure 2.31: Error in hairiness measurement

This is understandable because, at lower hairiness, the scattering is less making the output intensities low. At higher hairiness the error is less ($\sim$ 1%). The method can be performed with a natural light (white light) sources also. In fact this may result in better hairiness measurement as this type of light sources produce much higher light output intensities making the detection of scattered light easier and also resulting in a higher signal to noise ratio. Fig. 2.32 gives the variation in hairiness for 1m of the yarn, showing the random variation of hairiness. It is found that even for very small protruding fibers ($\sim$0 5 mm in length) noticeable variation in the output is observed. This makes the present method very accurate.

This method is tested using static yarns only. But the textile industry needs a dynamic method for hairiness measurement. The usual yarn speeds for parameter measurements in textile mills are several hundred meters per minute This needs a sampling rate of approximately 0 1 – 1 kHz (for sampling every centimeter) and this requires a photo-detector with a response time of approximately 1 ms. The photo-detector used in the present experimental technique has a rise time of 7μs, which makes it possible to have sampling rate of tens of kHz. Therefore by using an appropriate ADC and a PC, the method can be made both dynamic and fully automatic. At present, efforts are being made in this direction.

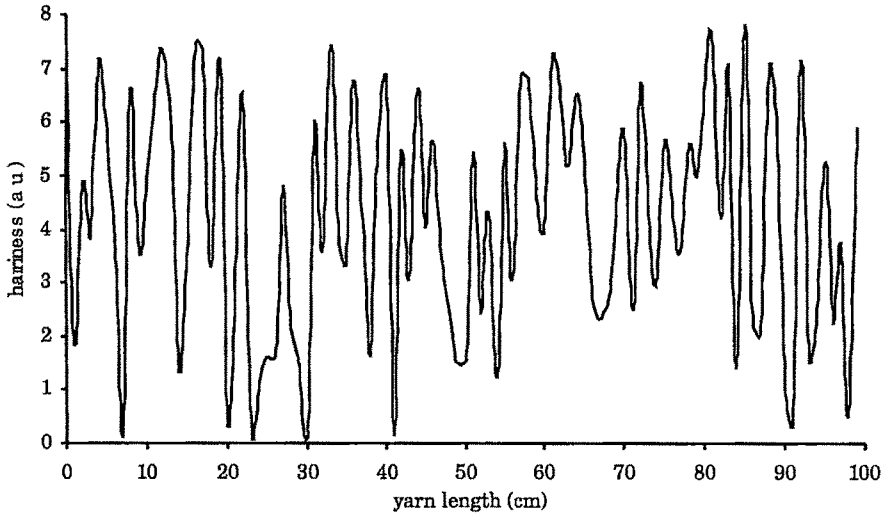

Figure 2.32: Variation in hairiness for 1m of the test yarn

2.2.4 Conclusion

A technique to measure hairiness in textile yarns is developed The measurement of the scattered light from the protruding fibers of the textile yarn yields the hairiness. Direct plane polarized beam is filtered out by a polarizer which allows only the scattered light (hairiness information) to pass. The method is found to be very accurate and sensitive.

2.3 Phase transition studies in Liquid Crystals using Laser Speckles

Liquid crystals are special materials in terms of their unique combination of factors namely flow properties of liquids and anisotropic properties of solids. Liquid crystalline phases represent fascinating states of soft matter, combining order and mobility on a molecular level This unique combination enables such systems to respond to external (magnetic, electric, chemical or mechanical) stimuli by finding a new configuration of minimum energy. Therefore liquid crystals are of great importance for numerous applications[67, 68].

Compounds when heated melt to clear liquids sharply at definite temperatures. Ther-

mal energy received by the molecules or atoms of a compound in a solid state make their bonds loose making them freely flowing isotropic liquids. However in liquid crystals this transition is not sharp. Several intermediate phases occur in such type of materials. This means that the liquid crystals do not melt in a single step from the anisotropic solid to the isotropic liquid state. The orientational and spatial ordering of these molecules characterize these intermediate phases[67]–[73]. The determination of this phase transition temperature is important for the potential applications of liquid crystals. Usually, the phase transition temperatures are identified using optical microscopy or thermal analysis. Recently a method using photon transmission has been developed to study phase transitions in liquid crystals[72, 73]. Here a new phase identification method for liquid crystals using laser speckle techniques is described. The speckle pattern is produced whenever coherent light is scattered from a surface whose roughness is comparable to or greater than the wavelength of the incident light[24, 74, 75]. The objective speckles from the scattering liquid crystal medium are used to determine the phase transition temperatures. In between the phase transitions, the liquid crystal exists as non ordered clusters resulting in high scattering and hence large number of speckles. Therefore by studying the variation of the speckle pattern with temperature, the phase transition of liquid crystals can be determined. Since speckle patterns can be regarded as arising from a large assembly of diffraction gratings of different line spacings and orientations, the structural change of the liquid crystal can also be investigated using this method.

2.3.1 Experimental setup and results

Experimental setup to study the phase transitions in liquid crystals is shown in Fig. 2.33. The source used is a He-Ne laser (10 mW, 633 nm). The laser beam is expanded using a spatial filtering assembly and is collimated using a collimating lens L This collimated beam is then passed through the liquid crystal sample mounted on a heating platform. The temperature is measured using a thermocouple sensor having a resolution of 0.1 ^{o}C. The light after passing through the sample falls on a semi-transparent screen. A CCD camera placed behind this screen records the images of the speckle patterns. The temperature is varied linearly with time. The speckle

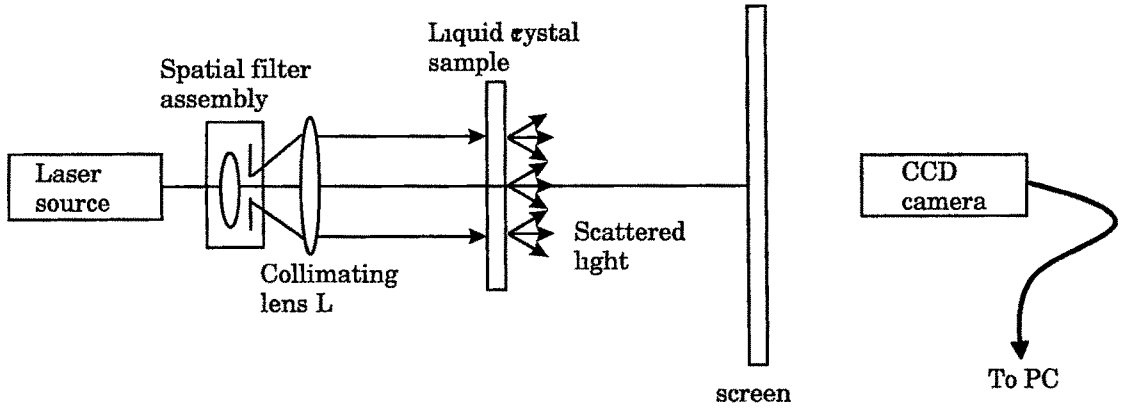

Figure 2.33. Experimental setup for studying phase transition studies in liquid crystals

pattern is recorded for every 0.1 °C rise in temperature.

Liquid crystals show a number of phases in between the solid and the isotropic phase. This means that these crystals do not melt in a single step during these transitions. In the most ordered form (solid state) the liquid crystal (LC) acts as a rough surface, forming speckles. Since the LC is in a solid form, the transmission is not high. So the number of speckles are less. As the liquid starts to form (semi-solid) the transmission increases, there are a large number of non-ordered clusters in this phase, scattering the incident coherent light thereby generating large number of speckles. Therefore this transition to semi-liquid/solid phase is indicated by a sudden increase in the number of speckles The scattering of the light can be determined from the number of speckles at the detector plane. The number of speckles is inversely proportional to the dark area at the detector plane and hence in the image. Therefore by measuring the number of dark pixels in the captured image at different temperatures the phase transitions can be identified.

The phase transition from the solid to semi-solid phase is indicated by a dip in the number of dark pixels (or raise in number of pixels). Then as the clusters combine together to form the first LC phase, the LC becomes ordered and there is a drastic reduction in the scattering of the incident light reducing the number of speckles. The increase in the number of speckles (or decrease in the number of dark pixels) at higher

(a) 25 °C (b) 45 °C (c) 55.4 °C

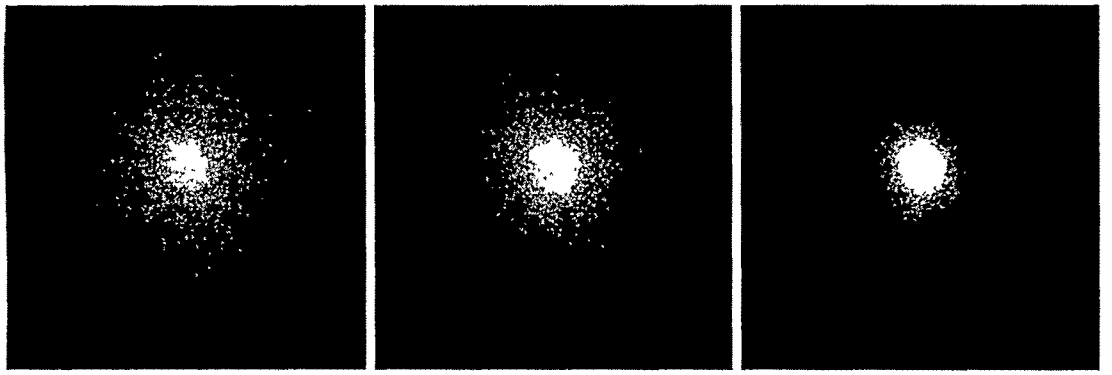

(d) 65 °C (e) 67 °C (f) 70 °C

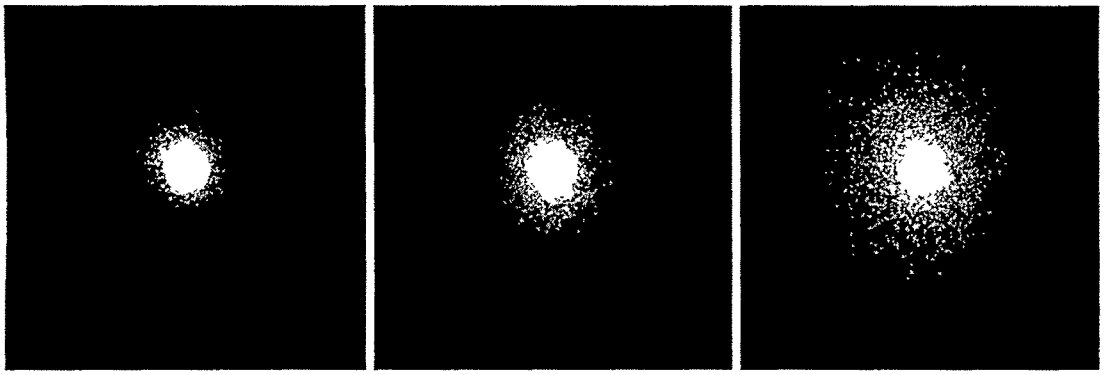

(g) 71.2 °C (h) 73 °C (i) 82 °C

Figure 2.34: Change in the speckle pattern with temperature for LC1

continued on next page

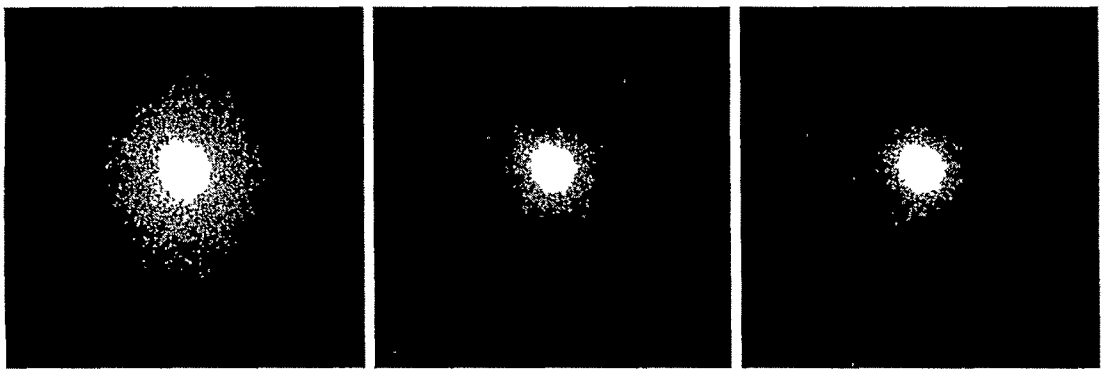

(j) 90 °C (k) 94.6 °C (l) 100 °C

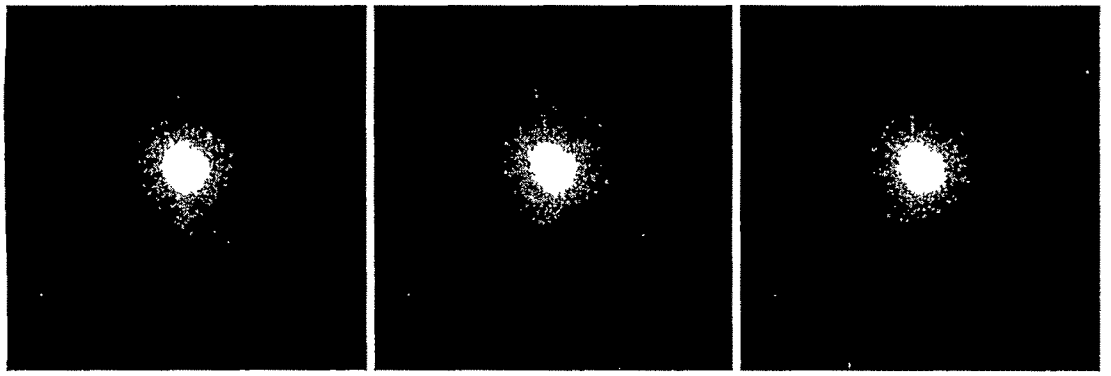

(m) 110.9 °C (n) 120 °C (o) 126.2 °C

Figure 2.34: Change in the speckle pattern with temperature for LC1

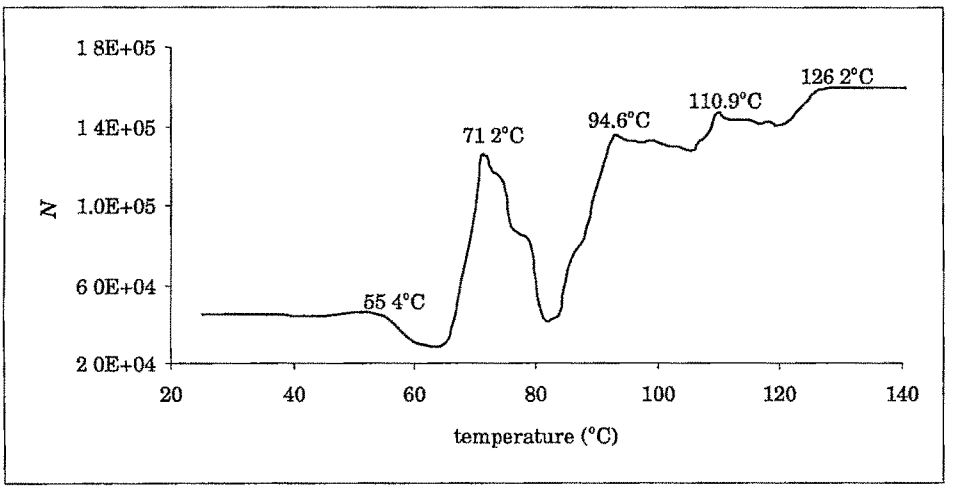

Figure 2.35: Change in the number of black pixels for LC1. Phase transition temperatures are marked

phase transition temperatures is less. This is because at higher temperatures the LC is mostly liquid, rather than solid, making the transmission high and number of speckles forming from the rough solid surfaces less. When the LC becomes isotropic (liquid state), there no longer will be any clusters inside the LC, resulting in no scattering and least number of speckles. By plotting the change in number of dark pixels with temperature, the phase transition temperatures can be identified.

Fig. 2.34 shows the change in number of speckles with temperature for the liquid crystal sample LC1 (4 - (4' - n - Dodecyloxybenzoyloxy) phenylazo- 4" - 1 - (3) - methylpropylbenzene)[76]. Liquid crystal (LC1) having four phase transitions found from optical microscopy and DSC. While in the solid form, LC1 is a rough surface with a low transmission, so the number of speckles are less (Fig. 2.34a, 2.34b). The solid to semi-solid transition is indicated by a sudden rise in the speckles because of scattering from large number of clusters (Fig. 2.34c). Fig. 2.35 shows the change in the number of black pixels with temperature for this LC. Here this phase transition is indicated by a dip in the number of dark pixels (around 55 °C). Then as the clusters combine together to form the first LC phase, the LC becomes ordered and there is a drastic reduction in the number of speckles (Fig. 2.34d-2.34g). The first phase transition occurs at 71.2 °C (Fig 2.34g). But after this phase transition, the LC again starts breaking into clusters increasing the number of speckles (72-83 °C in

Table 2.5: Phase transition temperatures of LC1

Phase	Transition temperature °C		
	Scattering	DSC	Optical microscopy
Crystal-Crystal	55.4	—	—
Smetic C*	71.2	72 4	73.1
Smetic A	94.6	94.1	92 4
Nematic	110.9	109.2	110
Isotropic	126.2	128.1	130.7

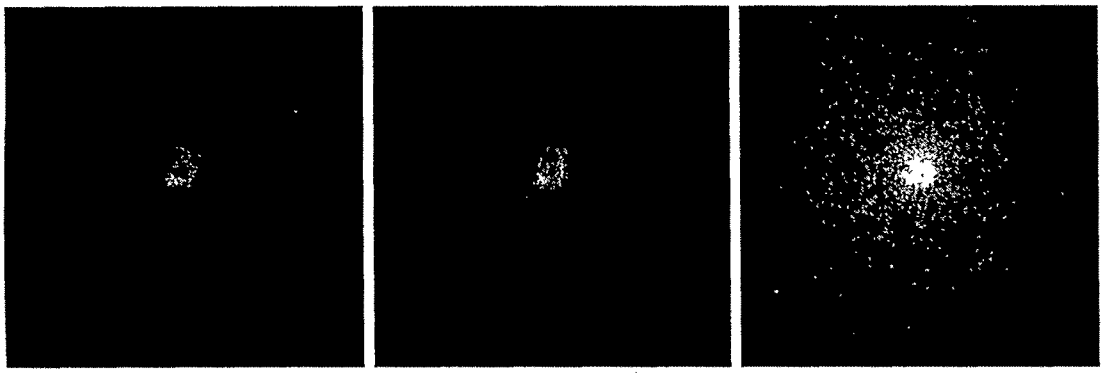

(a) 35 °C (b) 50 °C (c) 60.2 °C

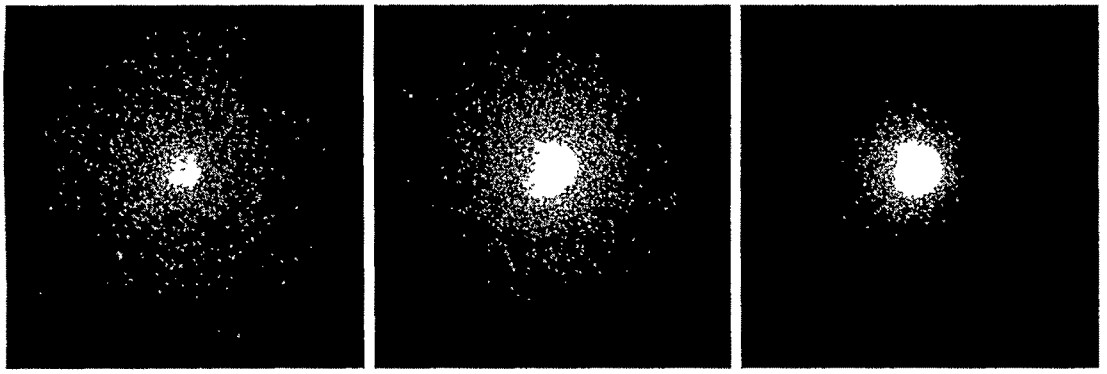

(d) 70 °C (e) 75 °C (f) 77 °C

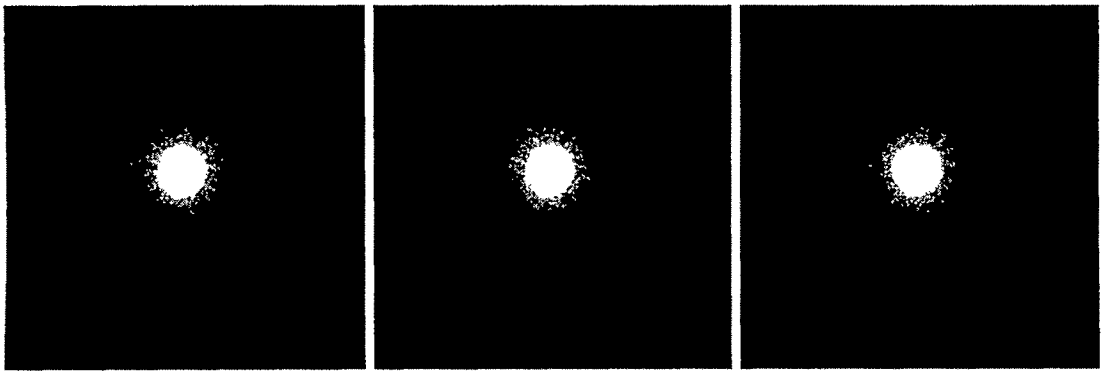

(d) 80 °C (e) 86.4 °C (f) 131.8 °C

Figure 2.36: Change in the speckle pattern with temperature for LC2

Fig. 2.34h-2.34i). The next phase transition begins at around 83 °C. This is indicated by a decrease in the number of speckles (Fig. 2.34j). The next phase transitions occurs at 94.6 °C and 110 °C respectively (Fig. 2.34k and Fig. 2.34m). At 126.2 °C,

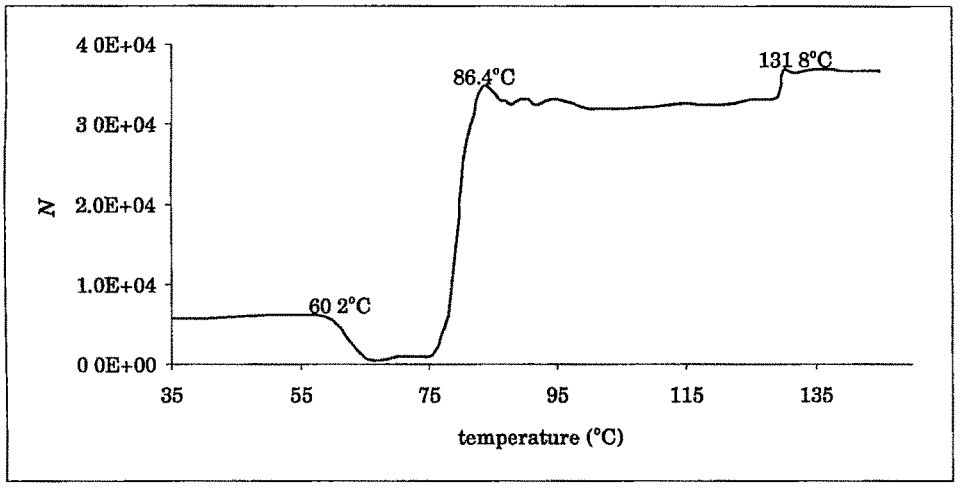

Figure 2.37: Change in the number of black pixels for LC2. Phase transition temperatures are marked

the LC becomes isotropic (liquid state, Fig. 2.34o). Here the number of speckles is least. Fig. 2.35 shows the change in number of black pixels with temperature. It can be seen that there is a sharp change in the number of speckles at the phase transition temperatures. From Fig. 2.35, it can also be seen that the change in number of speckles at higher phase transition temperatures are small compared with lower transition temperatures. Table 2.5 gives the obtained phase transition temperatures along with the transition temperatures obtained using differential scanning calorimetry (DSC) and optical microscopy. It can be seen that the results match very well.

Fig. 2.36 shows the variation in the speckle pattern for the second liquid crystal

Table 2.6: Phase transition temperatures of LC2

Phase	Transition temperature °C		
	Scattering	DSC	Optical microscopy
Unknown	60.2	—	—
Smetic C*	86.4	88.5	89.7
Isotropic	131.8	134.2	135.2

sample LC2. This sample was a mixture of 46 mol% of A3 (6 - methoxy - 2', 4" - dibenzoylerythromycin) in DBIA (4 - (4' - n - decycloxybenzoyloxy) - benzylidine-4"-isoamyloxyaniline)[67]. It has two phase transitions. Fig 2.36c shows the phase transition (crystal-crystal) at 60 2 °C, which is indicated by a sudden increase in the number of speckles. Fig. 2.36h shows the second phase transition at 86.4 °C At 131.8 °C the LC became isotropic (Fig. 2.36i). Fig 2.37 shows the change in number of black pixels with temperature for LC2. It can be seen that there are sharp changes at the temperatures where the phase transitions occur.

2.3.2 Conclusion

A new method which uses the objective speckle patterns arising from laser scattering from the liquid crystal sample is developed to study their phase transitions. The transition temperature determined using this method matches well with the transition temperatures measured using other methods. A new transition temperature (crystal-crystal) was also resolved using this technique. The method can be extended to study the structural properties of liquid crystal at transition temperatures. At present, work is going on to make the method more accurate.